Journal of Nanobiotechnology

RESEARCH

Open Access

A lyophilizable LNP vaccine enables STING-reinforced postoperational adjuvant immunotherapy

Yi Yang[1†], Jiaxin Guo[1†], Jialong Qi[2†], Wenxia Deng[1], Jialin Hu[1], Muhammad Waqqas Hasan[1], Fei Deng[3], You Zhou[1], Zhengji Song[2*], Wei Deng[4*] and Wenjie Chen[1*]

Abstract

Immune checkpoint blockade therapy (iCBT) has revolutionized cancer treatment, however, there is a low response rate, especially in treating postsurgical reoccurring tumors. Vaccine based immunotherapy can sensitize iCBT, but its development was largely hindered by inefficient delivery and high requirements of storage. In this study, the vaccine loaded with immunostimulant was employed to improve iCBT-based adjuvant postsurgical therapy. A lyophilized, antigen E7 peptide and manganese ion (Mn^{2+}) co-delivered tumor vaccine was developed based on lipid nanoparticles (EM@LNP). The vaccination efficacy was examined in both prophylactic and therapeutic schemes in murine subcutaneous models, the synergetic effect of vaccination combined with anti-PD-1 therapy was further investigated in post-operative tumor model. EM@LNP vaccination elicited effective $CD8^+$T cell response through modulating tumor immunosuppressive microenvironment and conferring immune memory, demonstrating potent immunization in both preventive and therapeutic schemes. What's more, EM@LNP vaccination orchestrated with iCBT, efficiently repressing tumor recurrence. Further mechanism studies using inhibitor for cells invitro and the investigation using $STING^{-/-}$ mice confirmed that the cGAS-STING signaling pathway activated by Mn^{2+} is indispensable for LNP vaccination and the coordination with iCBT-based adjuvant immunotherapy. In summary, this study shows a lyophilized LNP vaccine could significantly amplify iCBT efficiency, providing a translational strategy of adjuvant immunotherapy for treating postsurgical tumor recurrence.

[†]Yi Yang, Jiaxin Guo and Jialong Qi contributed equally to this work.

*Correspondence:
Zhengji Song
song4715@163.com
Wei Deng
wei.deng@uts.edu.au
Wenjie Chen
wenjie.chen1@hdr.mq.edu.au

Full list of author information is available at the end of the article

Graphical abstract

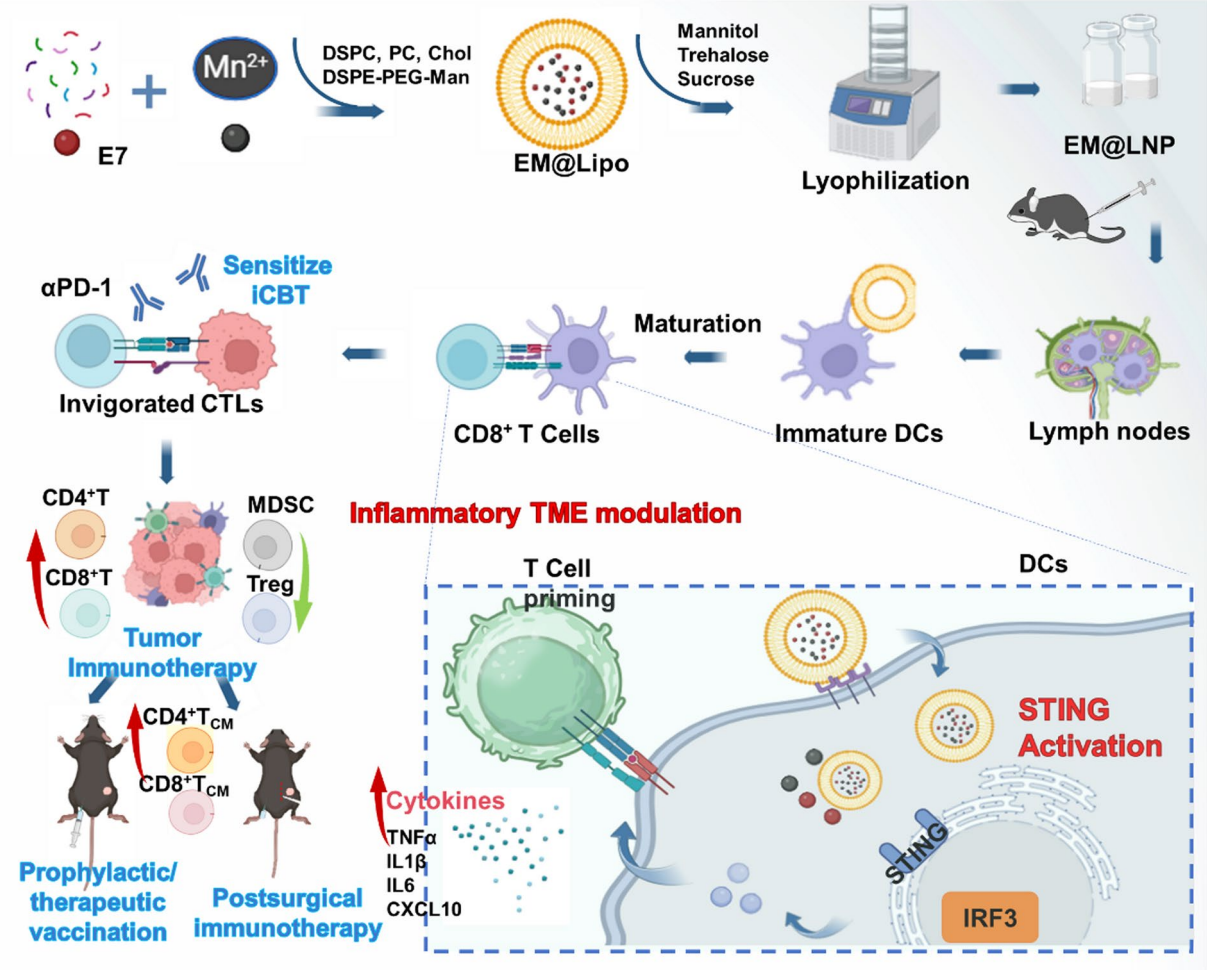

Keywords Lyophilizable LNP vaccine, iCBT, Adjuvant therapy, STING, Manganese

Introduction

Cancer immunotherapy represents an innovative approach that utilizes the autologous immune system to kill cancer cells [1]. A range of immunotherapeutic techniques have been integrated into clinical settings, including immune checkpoint blockade (ICB), adoptive T-cell transfer, oncolytic virus therapy, and therapeutic vaccines [2, 3]. These strategies have transformed conventional cancer treatment and offered new hope to patients with advanced-stage malignancies. Recently, the Food and Drug Administration (FDA) has granted approval to an expanding array of iCBTs. However, in "immunologically cold tumors", the paucity of immune cells infiltration limits the efficacy of iCBT in a subset of patients [4, 5]. Consequently, there is a pressing need for future clinical research to explore more potent combinatorial therapeutic approaches, with a particular focus on enhancing the responsiveness of immunologically cold tumors to immunotherapeutics.

The advancement of cancer vaccines marks a pivotal milestone in oncology, as they have the potential to stimulate the immune system especially the tumor-specific effector T cells to induce anti-tumor responses [6, 7]. HPV therapeutic vaccines, for instance, encompass a variety of forms such as subunit vaccines, nucleic acid vaccines, cell-based vaccines, synthetic peptide vaccines, and recombinant protein subunit vaccines [8]. Among them, HPV E7 protein stands out as a promising antigen capable of triggering specific anti-tumor cellular immune responses [9, 10]. Nevertheless, current trials have indicated that while E7-based cancer vaccine can elicit substantial $CD4^+$T response, while lacking robust $CD8^+$T cell responses [11]. $CD4^+$T cells are crucial in the immune process against exogenous antigens, facilitating

the interaction between T cell receptor (TCR) and antigen-MHC class II complex [12]; in contrast, $CD8^+$T cells are involved in the binding between TCR and antigen-MHC class I complex molecules [13, 14] and directly exert cytotoxic effects on cancer cells [15], there is an urgent need to develop reliable strategies to boost sufficient immunostimulation of E7 tumor vaccine.

The cGAS-STING signaling is a critical pathway of the innate immune regulatory mechanism that safeguarding cells against various pathogens and other immunostimulants [16–18]. This pathway functions through cytoplasmic DNA sensors, by detecting abnormal DNA, such as damaged DNA double-strand breaks (DSBs) or mitochondrial DNA that leaked into the cytoplasm [19]. STING activation is instrumental in spontaneous generation of anti-tumor T cell generation [20, 21]. STING agonists include cyclic dinucleotides (CDNs), the small molecule DMXAA, and metal ions [22]. Our group previously repurposed a statins drug lovastatin to increase DNA damage level and thus enhancing the chemodrug-induced STING activation [23]. Notably, manganese (Mn^{2+}) as an essential element for human physiology, plays a significant role in various biological processes, Mn^{2+} can augment the sensitivity of DNA sensor cGAS and its effector STING, thereby activating $CD8^+$T cells and natural killer (NK) cells [24, 25]. These properties render Mn^{2+} a promising candidate as an immune stimulant, with potential therapeutic applications in cancer immunotherapy.

Due to the fact that the components of vaccines are generally biomacromolecules, their delivery has always been one of the bottlenecks in maximizing the effectiveness of tumor vaccines [26, 27]. To achieve optimal regulation of anti-tumor adaptive immune regulation, it is essential to co-delivery adjuvants and antigens to lymphoid tissues [28, 29]. Lipid nanoparticles (LNPs) or the liposome form, with their cell membrane-like bilayer structure comprising a hydrophobic exterior and an encapsulated interior [30, 31], are utilized to co-encapsulate and deliver E7 and Mn^{2+}. Mn^{2+} acts as a vaccine adjuvant, can stimulate the cGAS-STING pathway [32], which facilitates antigen presentation and cytotoxic T lymphocyte (CTL) activation, thereby enhancing the anti-tumor immune response [33, 34].

Mn^{2+}-incorporated liposome platforms have recently gained attention for their ability to activate the cGAS-STING pathway to induce innate immunity and augment antitumor responses in chemo- and radio-therapy. For example, some recent work applied Mn^{2+}-incorporated liposomes to reverse doxorubicin chemoresistance [35] and attenuating hypoxia-induced radioresistance [36]. These platforms, while effective in enhancing immune sensitization to overcome chemo- or radio-resistance, primarily fail to induce adaptive immune responses necessary for vaccine-based long-lasting immunotherapy strategies. Another work developed a spleen-targeted mRNA vaccine (Mn@mRNA-LNP) for cancer immunotherapy [37]. The platform co-delivers mRNA antigens and Mn^{2+} directly to dendritic cells in the spleen, promoting their maturation and activating the STING signaling pathway, showing potent cytotoxic T cell responses and tumor suppression in melanoma and colon cancer models. However, this platform relies on a liquid formulation, which poses challenges for long-term stability, storage, and transportation—critical factors for clinical translation. Additionally, its emphasis on spleen targeting leaves a gap in addressing postsurgical tumor recurrence, a scenario that demands robust immune memory and modulation of the local tumor microenvironment. When used in the vaccination settings, it is vital to target the antigen presenting cells (APCs), particularly the dendritic cells (DCs), to effectively present antigens, and inducing generation of specific cytotoxic T lymphocytes [38, 39].

Most marketed vaccine products are aqueous dispersions with instability, which may need ultra-cold storage conditions. This is especially evident by the Pfizer-BioNTech and Moderna COVID-19 vaccines, which require storage temperatures at -80 °C and − 20 °C, respectively [40]. The stability of vaccines is a critical factor in their clinical translation, particularly when considering large-scale production, distribution, and storage. Traditional liquid vaccine formulations often require stringent storage conditions, including refrigeration or freezing, which increase transportation costs and present significant logistical challenges. These extreme storage requirements result in significant infrastructure and economic burdens, particularly in low-resource settings or regions with limited cold chain capabilities. Moreover, the instability of aqueous dispersions, particularly when subjected to temperature fluctuations or long-term storage, can lead to a loss of vaccine potency, further exacerbating these challenges.

In our work, we have developed a freeze-dried form of liposomes to deliver cancer vaccine agents, ensuring the stability of the lipid bilayer while addressing challenges such as aggregation, fusion and component leakage [41, 42]. Such lyophilized formulation can be directly used as solid dosage forms like sprays or reconstituted into suspensions, which ensure for long-term storage stability, and improve convenience of medication administration. This is particularly important in the treatment of postsurgical tumor recurrence, where timely and efficient vaccine administration is critical for achieving therapeutic success. These lyophilized liposomes were loaded with antigen peptide and Mn^{2+} for enhanced cancer iCBT and postsurgical adjuvant immunotherapy. To further improve the ability to target lymph node DCs, mannose is conjugated to the surface of the liposomes.

Mannose specifically targets DCs and has demonstrated anti-tumor and anti-metastatic properties, suggesting that a tumor vaccine could not only precisely target DCs but also potentially exert cytotoxic effects on tumor cells [43, 44]. Our EM@LNP vaccine effectively elicits $CD8^+$ T cell responses, modulates the immunosuppressive tumor microenvironment, and confers long-lasting immune memory. Furthermore, in combination with iCBT, this vaccine demonstrated significant efficacy in repressing tumor recurrence following surgical resection. Mechanistic studies using STING knockout models confirmed the essential role of cGAS-STING activation in mediating these therapeutic effects. By integrating stability, potent immunogenicity, and compatibility with adjuvant immunotherapy, our study offers a novel and translational strategy for addressing the critical challenge of postsurgical tumor recurrence.

Materials and methods

Materials

Distearoyl Phosphatidylcholine (DSPC) (S50960, Shanghai Yuan Ye), Phosphatidylcholine (PC) (Y46792, Shanghai Yuan Ye), Cholesterol (Chol) (S11040, Shanghai Yuan Ye), DSPE-PEG-2000 (S25991, Shanghai Yuan Ye), DSPE-PEG-mannose (SJ6784, Shanghai Yuan Ye). HPV_{16} $E7_{44-62}$ (^{44}QAEPDRAHYNIVTFCCKCD^{62}) was purchased from GL Biochem. $MnC_4H_6O_4{\bullet}4H_2O$ was purchased from Aladdin. Cell Counting Kit-8 (CCK8 kit) was acquired from Glpbio (GK10001, USA). Unless otherwise specified, all chemicals were obtained from commercial sources and used without further purification. DMEM medium, RPMI 1640 medium, penicillin/streptomycin (P/S), 0.25% trypsin-EDTA, phosphate buffered saline (PBS) and fetal bovine serum (FBS) were purchased from Gibco (USA).

Mice and cell lines

All cells were purchased from American Type Culture Collection (ATCC, USA). C57BL/6 mice (female, 4 weeks old) were obtained from the Guangdong Provincial Experimental Animal Center (Guangzhou, China) and $STING^{-/-}$ mice were gifted form Dr. Cunbao Liu from the Institute of Medical Biology, Chinese Academy of Medical Sciences (IMBCAMS). All the mice were raised in Specific Pathogen Free (SPF) animal facilities. All animal experiments were conducted in accordance with the guidelines provided by Guangzhou Medical University IACUC under the ethics approval GY-2022-188.

Table 1 The DLS characterizations (size, PDI) after reconstitution of the lyophilized EM@LNP prepared using various pre-freezing programs and cryoprotectants. *

Pre-freezing Programs Lyoprotectants	Liquid nitrogen freezing post freeze-thaw cycles (1)	Directly freezing in liquid nitrogen (2)	Programmed pre-freezing (3)
M + T + S (A)	**A1**: 747 nm, PDI = 0.578	**A2**: 395 nm, PDI = 0.385	**A3**: 160.4 nm, PDI = 0.271
M + T (B)	**B1**: 434.3 nm, PDI = 0.392	**B2**: 364.1 nm, PDI = 0.256	**B3**: 424.2 nm, PDI = 0.367

*Mannitol 1% (**M**), Trehalose 2% (**T**), Sucrose 2% (**S**)

1: Freeze in liquid nitrogen for 1 min, then thawed at 37℃ for 2 min, three freeze-thaw cycles

3: Temperature decreasing from 37℃ to -80℃ (rate = 1 ℃/min)

Preparation of EM@LNP vaccines

In briefly, liposomes were fabricated via the thin-film hydration technique. For the blank liposome devoid of loading any payload, DSPC, PC, cholesterol, DSPE-PEG2k, DSPE-PEG-Mannose was dissolved in chloroform/methanol solvent (V: V = 1:1). This mixture was then subjected to rotary evaporation under vacuum to remove the solvent for 1 h, resulting in a dried lipid film. The dried lipid film was subsequently rehydrated using PBS for 1 h. Then, monodispersed liposomes were obtained by extruding the suspension using an Avanti mini-extruder equiped with 200 nm polycarbonate filters. EM@LNP (liposome incorporating E7 and Mn^{2+}), E7@LNP (liposome incorporating E7) nanoparticles containing drugs were accomplished by incorporating the respective ingredients into the PBS during the hydration step, following the same procedures as described above.

EM@LNP was freeze-dried using a freeze dryer (Scientz-10ND, Ningbo) according to different pre-freezing programs as shown in Table 1. The as-prepared liposomes were designated as $EM@LNP_{fresh}$. Afterwards, the EM@LNP was characterized with a JEM-1400PLUS transmission electron microscope (TEM) for morphology examination, and the Malvern zetasizer (Nano-ZS90) for dynamic light scattering measurement. The encapsulation efficiencies of E7 and Mn^{2+} were determined by bicinchoninic acid (BCA) assay kit (20201ES76, Yeasen Bio.) and inductively coupled plasma mass spectrometry (ICP-MS), respectively.

In vitro cellular uptake

In vitro cell uptake was studied by confocal laser scanning microscopy (CLSM) and flow cytometry. For CLSM, DC2.4 cells were plated in glass-bottom dishes at a concentration of 1×10^4 cells. Then, free E7 (FAM-E7), $EM@LNP_{fresh}$,or EM@LNP were added to cells. After a series of incubation durations, cells were stained with Hoechst 33,342 (C1025, Beyotime) following the manufacturers' instructions. The cells were then visualized using a Zeiss LSM 800 confocal microscope. For flow cytometry, DC2.4 cells were seeded on 6-well plates, and then treated with FAM-E7. Post-incubation at various time intervals, cells were collected and rinsed twice in

preparation for analysis using a CytoFLEX Flow Cytometer (Beckman, USA).

Viability assay and activation of BMDCs

As previously described, bone marrow-derived DCs (BMDCs) were obtained from the tibia and fibula of female C57BL/6 mice, inoculated into 96-well plates at 1×10^5 cells/well, and incubated with different concentrations of EM@LNP for 24 h, respectively. Finally, the cell viability was detected using CCK8 cell viability kit.

The activation of DCs was evaluated by examining the expression levels of cytokines and cell surface markers. The BMDCs were incubated with PBS, LNPs, free E7, free E7 + Mn^{2+}, E7@LNP and EM@LNP for 24 h. The cytokine concentrations in the supernatants were measured with enzyme-linked immunosorbent assay (ELISA) according to a previously described method. Antibodies were provided by Elabscience Ltd., surface molecular expression of DCs was analyzed by flow cytometry using Pcy5.5-CD11c, PE-CD80, APC-CD86, APC-H-2Kb (MHC I), and FITC-CD40 antibodies. Data acquisition was performed using a CytoFLEX flow cytometer (Beckman, USA) and analysis was conducted using FlowJo software. The gating strategies applied are depicted in Supplementary Figures S4-5.

EM@LNP vaccine activated cGAS-STING pathway in BMDCs

BMDCs were treated separately with PBS, LNPs, free E7, free E7 + Mn^{2+}, E7@LNP, EM@LNP_{fresh}. and EM@LNP. Following treatment, cells were lysed using RIPA lysis buffer (20101ES, Yeasen Bio.) containing protease and phosphatase inhibitors (ST505, Beyotime). Protein extraction from cells was achieved by centrifugation at 12,000 rpm for 15 min. Protein concentration was determined using the BCA protein assay kit (20201ES, Yeasen Bio.). Subsequently, equal amounts of protein were separated on a 12% SDS-PAGE gel by electrophoresis (20326ES, Yeasen Bio.), and then transferred to a PVDF membrane (1620177, BioRad). The membrane was blocked for 1 h in a TBST buffer containing 5% blotting grade (P0216, Beyotime). After blocking, the membrane was incubated overnight at 4 °C with primary antibodies against Phospho-STING (72971, CST), Phospho-TBK1 (5483, CST), Phospho-IRF-3 (29047, CST), STING (13647, CST), TBK1 (38066, CST), and IRF-3 (4302, CST). The PVDF membrane was washed three times for 30 min each and incubated at room temperature with HRP-conjugated secondary antibodies (33101ES60, 33201ES60, Yeasen Bio.) for 2 h. Chemiluminescence was used to develop the protein bands with a gel imaging system (AI600), applying 200 μL of ECL chemiluminescent reagent (P0018S, Beyotime) was applied to the top of the membrane. Stripping buffer (P0025B, Beyotime) and the process was repeated. GAPDH (GB12002, Servicebio) was served as an internal loading control.

In vivo immunization and the flow cytometry assay of antigen-specific T cell response

C57BL/6 mice were immunized via subcutaneous injection with different formulations of vaccines on days 1 and 7: (1) PBS, (2) E7, (3) E7 + Mn^{2+}, (4) E7@LNP and (5) EM@LNP equivalent to the dose of E7 at 0.1 μg/mouse. On day 14, tumor challenge was conducted by subcutaneous inoculation with TC-1 tumor cells (1×10^6) on the right flank. Tumor sizes and body weight were tracked every two days. Tumor volume was calculated as Volume = (length× width× width)/2. On day 29, mice were euthanized, and lymphocytes from lymph nodes and spleen were extracted using PBS. These cells were then subjected to a lymphocyte separation process followed by analysis via flow cytometry.

Biodistribution and biosafety study

To assess the in vivo antigen stability and the pattern of EM@LNP migration to the draining LNs, C57BL/6 mice were subcutaneously (s.c.) injected with PBS, free FAM-E7, FAM-EM@LNP. The IVIS spectrum imaging system (PerkinElmer, USA) injected the FAM-labeled E7 signal at the immunization site under the conditions of the excitation filter of 470 nm and emission filter of 535 nm. Six hours after immunization, major organs including heart, liver, spleen, lung, kidney, and inguinal lymph nodes were obtained from sacrificed mice for ex vivo FAM fluorescence imaging.

In vivo tumor models and combination iCBT

C57BL/6 mice were subcutaneously injected with TC-1 cells (1×10^6) on the right flank. On day 7, mice were randomly divided into 6 groups ($n = 6$) and vaccinated with (1) PBS, (2) αPD-1, (3) E7 + Mn^{2+}, (4) EM@LNP, (5) E7 + Mn^{2+} + αPD-1, (6) EM@LNP + αPD-1 equivalent to the dose of E7 at 1 μg/mouse and αPD-1 (i.p. 100 μg/mouse). Vaccines were subcutaneous injection on days 8 and 15. Again, mouse αPD-1 (BE0146, BioXcell) were administered intraperitoneally on days 9 and 16, followed by monitoring tumor volume and body weight monitoring as above. Mice were euthanized if the tumor volume exceeded 2,000 mm^3. On day 24, mice were sacrificed, tumors, spleens, and LNs were collected for the following analysis.

Gene expression in the tumor microenvironment

Tumor RNA was isolated with TRIeasyTM reagent (10606ES, Yeasen Bio.). cDNA synthesis was performed using a cDNA synthesis kit (11142ES, Yeasen Bio.). β-actin was used as the reference gene. The expression of target genes was evaluated using RT-qPCR with StepOne

Plus instrument (BI, USA) and SYBR Green reagent (11203ES, Yeasen Bio.). Primer sequences can be found in Supplementary Table S1. Tumor protein was analyzed as described in 2.6.

Postsurgical tumor model and combination immunotherapy

A density of 1×10^6 TC-1 cells were subcutaneously injected into C57BL/6 mice on right flank, 11 days after inoculation, anesthetized the mice and the tumors were resected with sterile instruments, leaving about 20 mm^3 of residual tumor tissue. Three days after surgery, tumor volume and body weight were monitored as above. On day 17, mice were randomly divided into 4 groups ($n = 6$) and treated with (1) PBS, (2) αPD-1, (3) EM@LNP, (4) EM@LNP + αPD-1 equivalent to the dose of E7 at 1.5 μg/mouse. Vaccinations were done by subcutaneous injection on days 17 and 24. For ICB combination therapy group, mouse αPD-1 was administered intraperitoneally on days 18 and 25. Mice were euthanized when the tumor volume exceeded 2,000 mm^3.On day 33, mice were sacrificed, tumors, spleens, and LNs were collected for the following immune analysis.

STING$^{-/-}$ mice tumor models and combination iCBT

STING knockout mice were subcutaneously injected with TC-1 cells (1×10^6) on the right flank. On day 7, mice were randomly divided into 6 groups ($n = 6$) and vaccinated with (1) PBS, (2) αPD-1, (3) E7@LNP + αPD-1, (4) EM@LNP + αPD-1 equivalent to the dose of E7 at 1.5 μg/mouse. Vaccines were subcutaneously injected on days 8 and 15. Again, mouse αPD-1 (BE0146, BioXcell) were administered intraperitoneally on days 9 and 16, followed by monitoring tumor volume and body weight monitoring as above. Tumor volume was calculated as (length× width× width)/2. On day 24, mice were sacrificed, tumors, spleens, and LNs were collected for the following analysis.

Flow cytometric analysis of tumor immune microenvironment

Tumors, lymph nodes, and spleens were harvested and processed for assessment of the anti-tumor immune response via flow cytometry using the CytoFLEX platform. In brief, the collected tissues were dissociated into single-cell suspensions, and red blood cells were lysed using a red blood cell lysis buffer (R1010, Solabio). The cells were then blocked with 0.1% BSA (36101ES, Yeasen Bio.) in PBS followed by a 1-hour incubation with specific antibodies at room temperature. For the characterization of T cells and DCs in tumors and spleens, staining was performed using anti-mouse CD3-Pcy5.5 (F1013J, Elabscience), anti-mouse CD4-FITC (F1097C, Elabscience), anti-mouse CD8a-PE (F1104D, Elabscience), anti-mouse CD11b-FITC (F1081C, Elabscience), anti-mouse Gr-1-PE (F1120D, Elabscience), anti-mouse IFN-γ-APC (F1101E, Elabscience), anti-mouse Foxp3-PE (F1238D, Elabscience), anti-mouse CD62L-Pcy5.5 (F1011J, Elabscience) and anti-mouse CD44-APC (F1100E, Elabscience). Data acquisition was performed using CytExpert software, and analysis was conducted using FlowJo software. The gating strategies are detailed in Supplementary Figures S8-10.

Immunohistochemistry (IHC) and immunofluorescence (IF)

The tumor tissue sections were stained with hematoxylin and eosin (H&E) and TUNEL to detect histological changes. For IHC analyses on immune cell infiltration, the tissue sections were incubated with an anti-CD8 or anti-Foxp3 antibody (Servicebio). Finally, images were photographed using fluorescence microscopy (Nikon).

Statistical analysis

All quantitative values are reported as the mean ± standard error of the mean (SEM). Data were evaluated by one- or two-way analysis of variance (ANOVA) for comparison of multiple groups using GraphPad Prism 5 software. $^*p < 0.05$, $^{**}p < 0.01$, $^{***}p < 0.001$ were considered as significant difference.

Results

Preparation and characterization of EM@LNP

To simultaneously deliver E7 and Mn^{2+}, EM@LNP was prepared for their co-encapsulation. As delineated in the Scheme 1, EM@LNP_{fresh} was synthesized successfully and TEM images showed that EM@LNP_{fresh} had an average diameter of about 200 nm, with a uniform spherical morphology (Fig. 1A). Further analysis by dynamic light scattering revealed that the average particle size of EM@LNP_{fresh} was 152.5 nm, with a PDI of 0.201. The zeta potential of EM@LNP_{fresh} was around − 14 mV (Fig. 1B). The encapsulation efficiency of E7 was found to be 85 ± 4%, with a drug loading rate of 3.2 ± 0.1%. Similarly, the encapsulation efficiency of Mn^{2+} was determined to be 99.8%, with a drug loading capacity of 9.4% (Figure S1). By using different pre-freezing programs and lyoprotectant combinations, the particle size analysis by dynamic light scattering indicated that the optimal size for freeze-dried liposomes using program A3 (with ternary lyoprotectant of mannitol + trehalose + sucrose, programmed prefreezing) was around 160.4 nm (Table 1), with a PDI value of 0.271 (Fig. 1C), and the zeta potential was approximately − 18.7 mV (Fig. 1D), which closely resembled with the original liposome particles in terms of size and potential. TEM images also confirmed the uniform spherical morphology (Fig. 1E). The freeze-dried LNPs prepared using program A3 exhibited excellent thermal stability, as evident from thermogravimetric (TG) assay

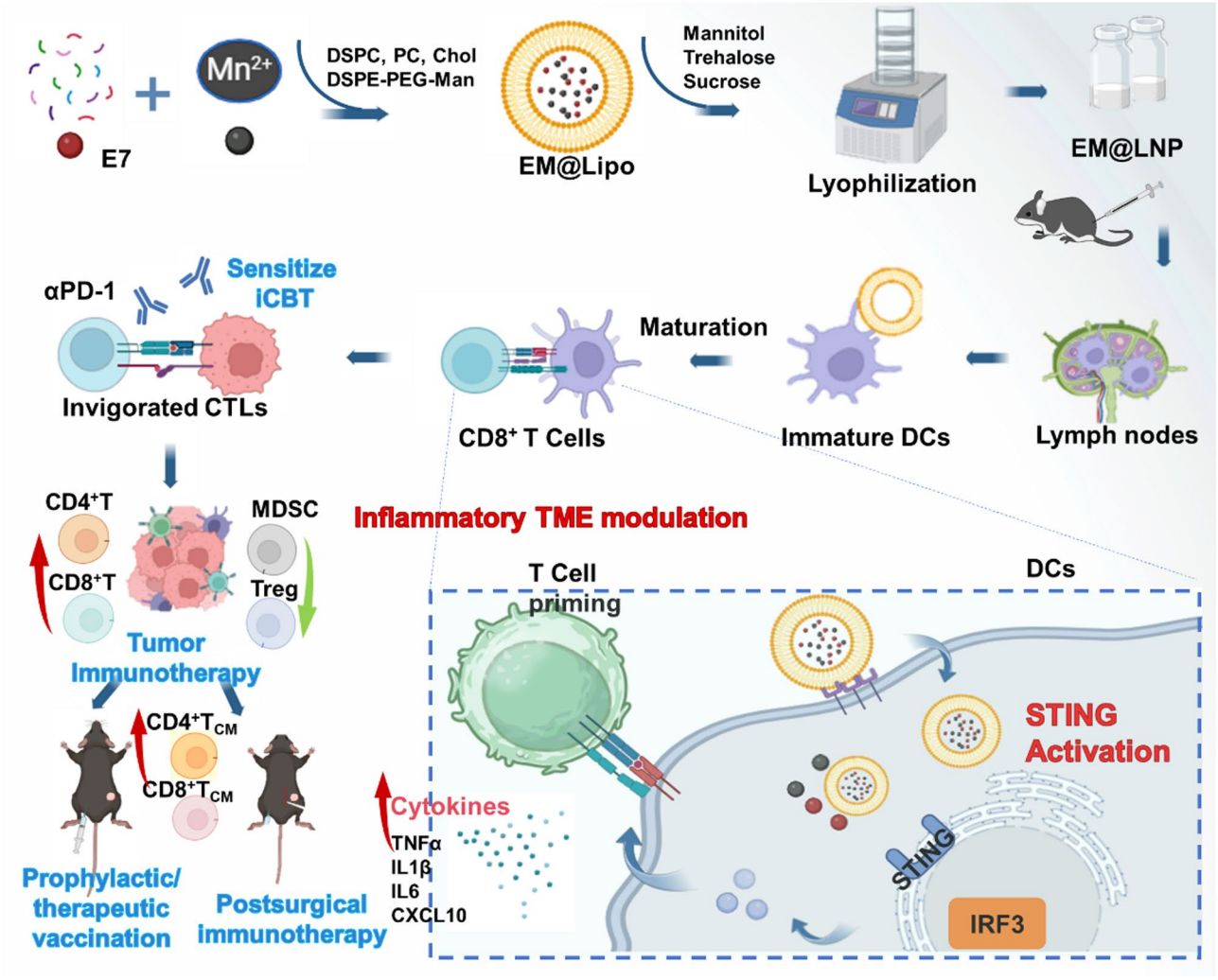

Scheme 1 The schematic diagram of this study. It illustrates the preparation of the lyophilized LNP vaccine loaded with E7 peptide and Mn^{2+} for promoting DC maturation and specific T cell immune response by activating STING pathway and modulating the TME from immunosuppressive to inflammatory, thus leading to robust cancer vaccination and amplified iCBT for postsurgical immunotherapy to eliminate the tumor recurrence

in Fig. 1F, only 10% of mass loss were observed at 100 ℃ and no more than 25% of mass loss at 200 ℃.

EM@LNP promoted BMDC maturation through cGAS-STING pathway

After incubating EM@LNP with BMDCs at different concentrations for 24 h, cell viability was analyzed. The findings indicated that E7 exhibited no significant cytotoxicity when the concentration of EM@LNP was less than 5 mg/mL (Fig. 2A), indicating an excellent safety within a certain range. Furthermore, confocal and flow cytometry data demonstrated that EM@LNP significantly improved cellular uptake, suggesting that LNPs encapsulation can facilitate vaccine delivery, and the same effect was achieved before or after the lyophilization of LNP (Figs. 2B-C, S2-3). The activation and maturation of BMDCs stimulated by EM@LNP were evaluated by flow cytometry to measure the expression levels of maturation markers CD80, CD86, CD40 and MHC II. Moreover, there was no significant difference between the lyophilized EM@LNP and the fresh EM@LNP in the potentiation effect of BMDCs maturation (Fig. S6A-D) and the secretion of cytokines including TNF-α, IL-1β and IFN-β (Figure S6E), respectively. The comparisons of lyophilized LNP with the freshly-prepared LNP demonstrate that lyophilization did not affect the biological effect of EM@LNP, hence, in the subsequent studies, lyophilized EM@LNP was used after reconstitution. The results showed that EM@LNP significantly promoted the expression of surface markers and stimulated BMDCs maturation (Fig. 2D-G). In addition, ELISA analysis of cytokine levels revealed that EM@LNP enhanced secretion of TNF-α (Fig. 2H), IL-1β (Fig. 2I), IFN-γ (Fig. 2J) and IFN-β (Fig. 2K), indicating that the addition of STING agonist Mn^{2+} significantly enhanced the capability of BMDCs maturation. Subsequent experiments were conducted to

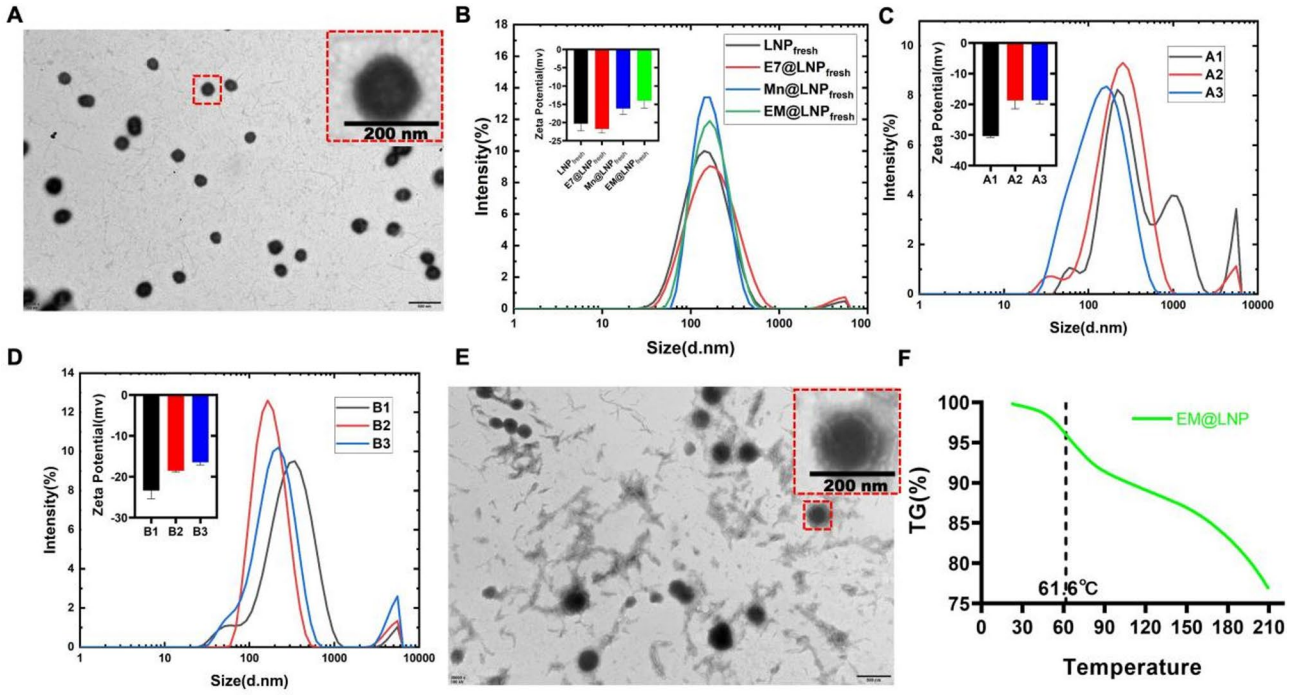

Fig. 1 Characterizations of freeze-dried EM@LNP. (**A**) Representative TEM image of EM@LNP$_{fresh}$. (Scale bar: 200 nm) (**B**) Hydrodynamic diameter and potential values measured by DLS. (**C**) Hydrodynamic diameter images and (**D**) potential value of EM@LNP with different freeze-drying methods. (**E**) Representative TEM image of LNPs after reconstitution using the freeze-dried method A3. (Scale bar: 200 nm). (**F**) TG analysis graph of EM@LNP

further verify whether the activation of cGAS-STING pathway expression by Mn^{2+} could enhance its anti-tumor effect. BMDCs and TC-1 cells were first incubated in PBS, free LNPs, E7, E7 + Mn^{2+}, E7@LNP or EM@LNP for 24 h, after which proteins related in cGAS-STING pathway were analyzed. Western-blot results showed that EM@LNP increased the expression of phosphorylated TBK1, STING and IRF3, with no significant changes in the overall levels of these proteins (Fig. 2L-M). In addition, when STING inhibitor H-151 led to a decrease in TBK1, STING, and IRF3 expression levels, demonstrating that EM@LNP's anti-tumor effects are mediated through a cGAS-STING pathway-dependent mechanism (Fig. 2N). Collectively, these findings advance our comprehension of how Mn^{2+} enhances the activation of cGAS-STING pathway for antitumor effects and provide important reference basis for developing new immunotherapy strategies.

Prophylactic immunization using EM@LNP prevented tumor occurrence and trained immune memory

In the subcutaneous tumor model utilizing TC-1 cells for a study of preventive immunization (Fig. 3A), mice vaccinated with EM@LNP displayed markedly reduced tumor growth compared to the control groups that received E7 + Mn^{2+}, E7@LNP and PBS. The addition of Mn^{2+} further augmented the immunosuppressive effect, particularly in the EM@LNP group where tumor growth was almost completely suppressed, with 2/3 of the mice showing tumor regression (Fig. 3B-C). On day 29, the tumors' weight revealed that the mice vaccinated with E7 had a significant reduction in both tumor volume and weight compared to the control groups (Fig. 3C), with the EM@LNP group exhibited the lowest tumor occurrence of 33% (Fig. 3D), suggesting the best protective effect. Additionally, while spleen weight corresponded with these changes, the body weight of the mice remained stable throughout the immunization period (Figure S7). These findings indicate that EM@LNP incorporating STING agonist Mn^{2+} possesses the strongest potency as prophylactic vaccine to prevent tumor development. Notably, the robust antitumor response observed with the E7 + Mn^{2+} physical mixture underscores the critical role of Mn^{2+} in enhancing immune activation; however, the superior protective effect of EM@LNP suggests that the LNP formulation further optimizes antigen delivery and immune stimulation. To confirm the impact of the STING agonist Mn^{2+} adjuvant on the TME, spleen and lymph node tissues, the immune cell populations were analyzed using flow cytometry. The results showed that tumor-suppressive immune response was significantly reversed in mice immunized with EM@LNP. Compared to the control group, there was a notable increase in the proportion of CTLs ($CD8^+IFN\gamma^+$) in $CD8^+$ cells in mice immunized with E7 + Mn^{2+} or EM@LNP, with an even more pronounced effect observed in the EM@

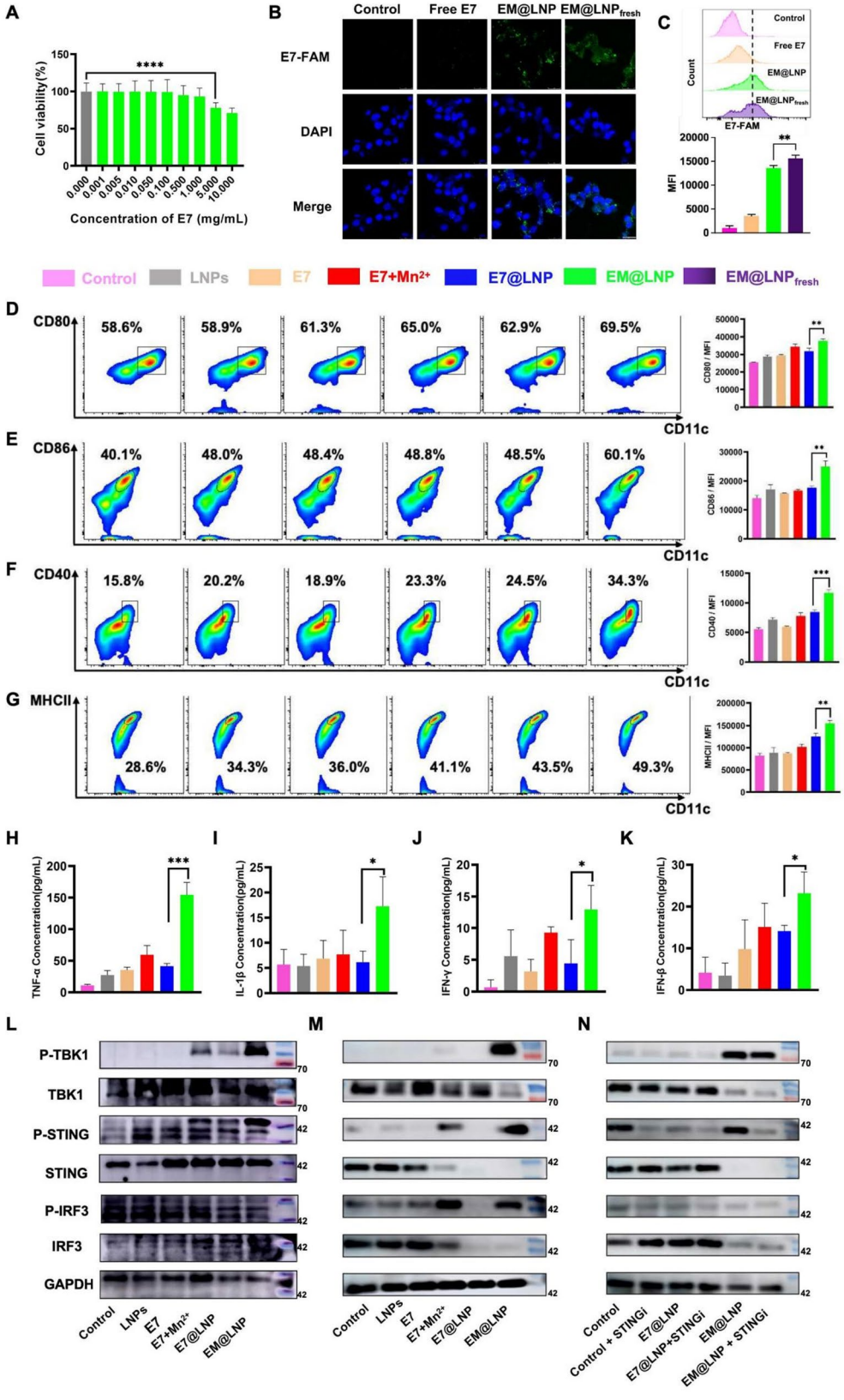

Fig. 2 (See legend on next page.)

(See figure on previous page.)

Fig. 2 EM@LNP enhanced cellular uptake of antigen and promote the maturation of BMDCs. (**A**) Relative cell viability assay in BMDCs. (**B**) Confocal images showing cellular uptake after 12 h of incubation. (Scale bar: 25 μm) (**C**) Flow cytometry analysis of cellular uptake after 12 h of incubation. (**D**) Representative flow cytometry plots and statistical analysis for CD80. (**E**) Representative flow cytometry plots and statistical analysis for CD86. (**F**) Representative flow cytometry and statistical analysis for CD40. (**G**) Representative flow cytometry plots and statistical analysis for MHC II. (**H**) Secretion profile of the TNF-α cytokine, (**I**) IL-1β cytokine, (**J**) IFN-γ, and (**K**) IFN-β cytokine. (**L**) Western blotting of proteins TBK1, STING, and IRF3 in for BMDCs, (**M**) TC-1 cells after different treatments and (**N**) in TC-1 cells treated with STING inhibitor. Data are presented as mean ± SD. Statistical significances between every two groups were calculated via one-way ANOVA. *$p < 0.05$, **$p < 0.01$, ***$p < 0.001$

LNP group. Additionally, EM@LNP induced a significantly greater generation of central memory T cells (T_{CM}, $CD8^+CD44^+CD62L^+$ and $CD4^+CD44^+CD62L^+$) (Fig. 3E, S11). Further analysis of $CD8^+$ cells in lymph nodes revealed that after EM@LNP immunization, the frequency of CTLs was highest among $CD8^+$ cells, and a larger number of T_{CM} cells were generated (Fig. 3F, S12). In conclusion, using STING agonist Mn^{2+}-adjuvanted formulation elicited stronger E7-specific effector and memory T cell responses, ether in the group treated with LNP formulation (EM@LNP) or even the simple mixture ($E7 + Mn^{2+}$). Collectively, these findings highlight the significant role of the STING agonist Mn^{2+} in stimulating an immune response within the tumor-suppressive immune TME and demonstrate that the EM@LNP formulation offers enhanced antigen delivery and prolonged immune activation, leading to superior tumor prevention.

EM@LNP sensitized and intensified iCBT by reshaping TME

The above results indicate that the addition of Mn^{2+} can trigger the cGAS-STING activation, boosting immune responses within tumor tissues and increase responsiveness to iCBT. To delve deeper into the therapeutic potential of the combination of αPD-1 and the EM@LNP vaccine, a comprehensive set of experiments was undertaken (Fig. 4A). EM@LNP vaccine treatment was found to significantly inhibit tumor growth compared to mixture treatment. Particularly, even greater inhibition of tumor growth was observed when this treatment was combined with iCBT (Fig. 4B-C). Examination of tumor growth curves (Fig. 4D), along with assessments of changes in tumor weight and spleen weight, further corroborated these observations. In addition, the maintenance of stable body weight in mice indicated the safety of using EM@LNP and αPD-1 combination application, while EM@LNP + iCBT significantly extended the survival of the mice (Figure S13). These findings suggest that the Mn^{2+}-added LNP vaccine, EM@LNP remarkably enhances the anti-tumor response of iCBT.

By analyzing the tumoral infiltration of immune cells through IHC staining, compared to other groups, the EM@LNP + αPD-1 treatment showed more nuclear dissolution and apoptotic areas in H&E staining images (Fig. 5A). TUNEL assay revealed that the DNA damage rate was highest in the EM@LNP + αPD-1 immunized group (Fig. 5B), additionally, there was an increase in $CD8^+$ T cells and a decrease in Tregs ($Foxp3^+$) p (Fig. 5C-D). This implies that the treatment strategy effectively boosts anti-tumor effector cells while curbing the activity of immunosuppressive cells. A sequential increase in the response of anti-tumor effector cells was observed from the $E7 + Mn^{2+}$, EM@LNP, $E7 + Mn^{2+}$ + αPD-1 to EM@LNP + αPD-1, reflecting an escalating therapeutic efficacy. It is worth noting that key effector cells were significantly enhanced within tumors of mice treated with EM@LNP + αPD-1, particularly an elevated frequency of CTLs ($CD8^+IFN\gamma^+$) among $CD8^+$ lymphocytes and a substantial reduction in Tregs ($CD4^+$ $Foxp3^+$) (Figure S14). These results suggest that EM@LNP synergized-iCBT has promise as a potent anticancer vaccine, capable of augmenting the activity of key effector immune cells within tumors and suppressing immunosuppressive cells.

When contrasted with the control group of $E7 + Mn^{2+}$ and EM@LNP immunized mice, it was found that combined iCBT notably amplified the systemic response of key effector cells in the vaccinated mice. Specifically, injection of EM@LNP + αPD-1 activated anti-exhaustion cells and initiated $CD8^+$ T cells as well as increased memory T cells. Meanwhile, immunosuppressive MDSCs were observed reduced in splenocytes, and splenic Tregs in $CD4^+$ cells were significantly reduced, indicating a shift towards systemic immune response of antitumor effector cell reaction (Fig. 4E, S15). In addition, antigen-specific activation was identified to foster the maturation of immune cells within lymph nodes simultaneously (Fig. 4F, S16). These findings uncover the transformations among various immune cell types subsequent to various treatment regimens.

Western blotting analysis of tumor tissue samples was found that EM@LNP + αPD-1 treatment promotes phosphorylation of cGAS-STING pathway-related proteins, significantly activating the cGAS-STING pathway (Fig. 5F), enhancing the secretion of inflammatory factors and strengthening anti-tumor effects. Meanwhile, RT-PCR using the tumor tissue showed that compared to the control group, treatment with EM@LNP + αPD-1 significantly increased the relative expression levels of IFN-I (e.g., IFNB), inflammatory cytokines and chemokine genes in tumor tissues, such as TNF-α and Cxcl10 (Fig. 5E). Furthermore, investigation into macrophage polarization revealed that in the EM@LNP + αPD-1 treatment group, biomarkers representing M1-like macrophages TNF-α and IL-6 were significantly upregulated,

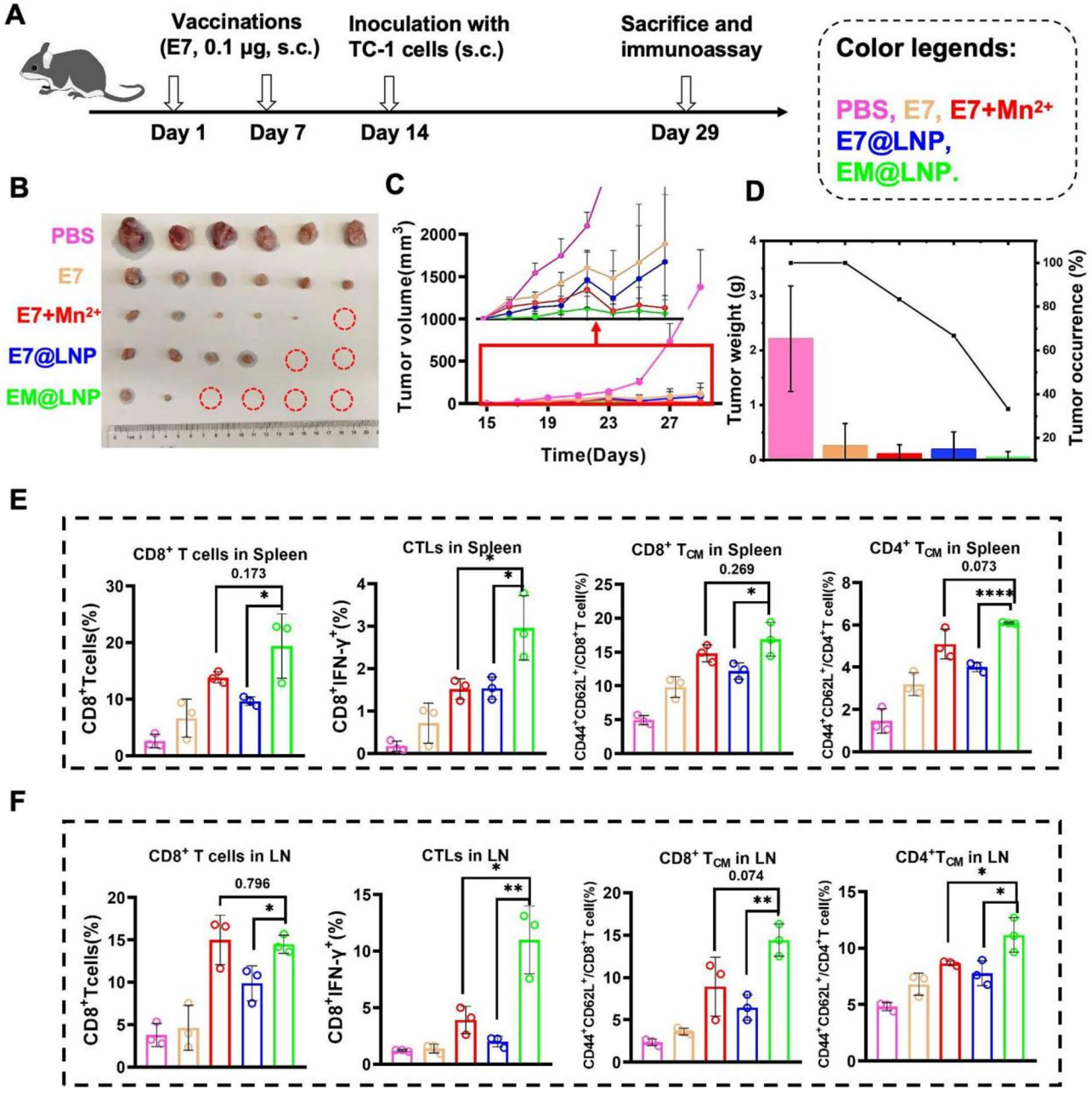

Fig. 3 EM@LNP effectively prevented tumor development in the prophylactic vaccination scheme. (**A**) The schematic illustration outlining the sequence of drug administration and assays. (**B**) The photographs of the tumor obtained at the therapeutic endpoint with various treatments. The dashed circles represent those mice without tumor occurrence. ($n = 6$) (**C**) Tumor growth curve, with an inset showing the zoom-in area. (**D**) Tumor weight of mice and cancer occurrence rate. (**E**) Flow cytometry analysis of immune cells in the spleen, including $CD8^+$T cells, CTLs ($CD8^+IFN\text{-}\gamma^+$), $CD8^+$ T_{CM} ($CD8^+CD44^+CD62^+$), and $CD4^+$ T_{CM} ($CD4^+CD44^+CD62^+$) cells. (**F**) Flow cytometry analysis of immune cells in lymph nodes. Data are presented as mean ± SD. Statistical significances between every two groups were calculated via one-way ANOVA. $^*p < 0.05$, $^{**}p < 0.01$, $^{***}p < 0.001$

thereby promoting the generation of an inflammatory environment within tumors.

To ascertain the biodistribution and biosafety of EM@LNP, FAM-labeled EM@LNP was injected subcutaneously into mice along with PBS and E7 + Mn^{2+}. An in vivo imaging system was utilized to track fluorescence signals. The results showed that the fluorescence intensity gradually increased at lymph nodes and tumor sites over time after injection of EM@LNP, reaching a peak at 24 h. Subsequently, the fluorescence intensity gradually decreased. These findings indicate that within 48 h, EM@LNP could effectively accumulates in tumors and lymph nodes (Figure S17). The physiological and biochemical parameters was assessed, along with histological

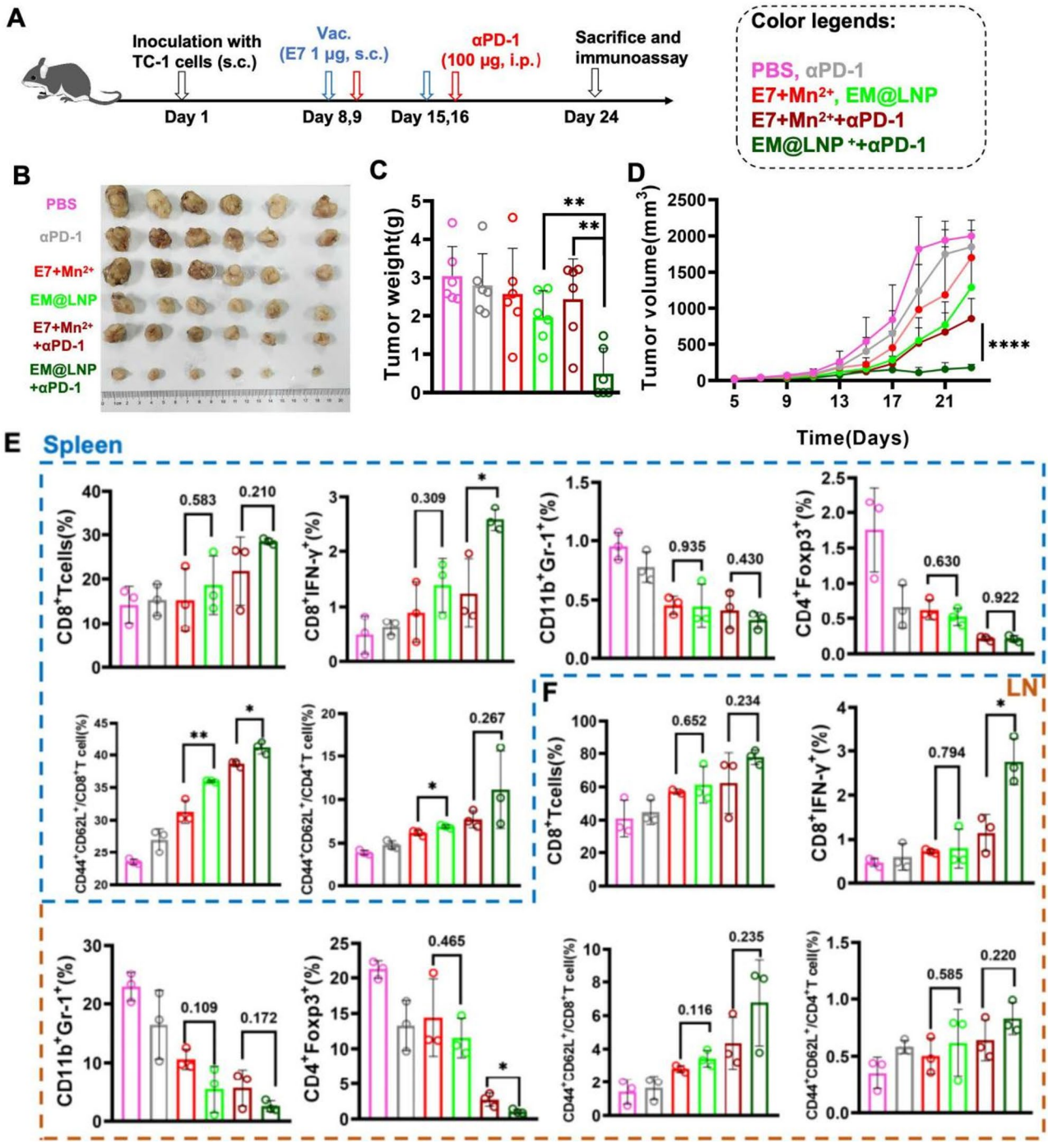

Fig. 4 EM@LNP in combination with iCBT significantly inhibited subcutaneous TC-1 tumor growth. (**A**) The schematic illustration outlining the sequence of drug administration and assays. (**B**) The photographs of the tumors obtained at the endpoints ($n = 6$). (**C**) Tumor weight of mice. (**D**) Tumor growth curve of each group. (**E**) Flow cytometric analysis of splenic immune cells, including $CD8^+$T cells, CTLs ($CD8^+IFN\text{-}\gamma^+$), MDSCs ($CD11b^+Gr\text{-}1^+$), Tregs ($CD4^+Foxp3^+$), $CD8^+$ T_{CM} ($CD8^+CD44^+CD62^+$), and $CD4^+$ T_{CM} ($CD4^+CD44^+CD62^+$) cells. (**F**) Flow cytometric analysis of immune cells in lymph nodes. Data are presented as mean ± SD. Statistical significances between two groups were calculated via one-way ANOVA. $^*p < 0.05$, $^{**}p < 0.01$, $^{***}p < 0.001$

examinations of organs. The blood biochemical analyses encompassing five different markers, demonstrated that mice administered with EM@LNP-treated treatment mice had values within normal ranges. Additionally, H&E staining of major organs (heart, liver, spleen, lung, kidney) of from mice given various treatments revealed no significant deviations from the morphology of organs in PBS-treated mice (Figure S18). These observations collectively confirm the satisfactory biosafety

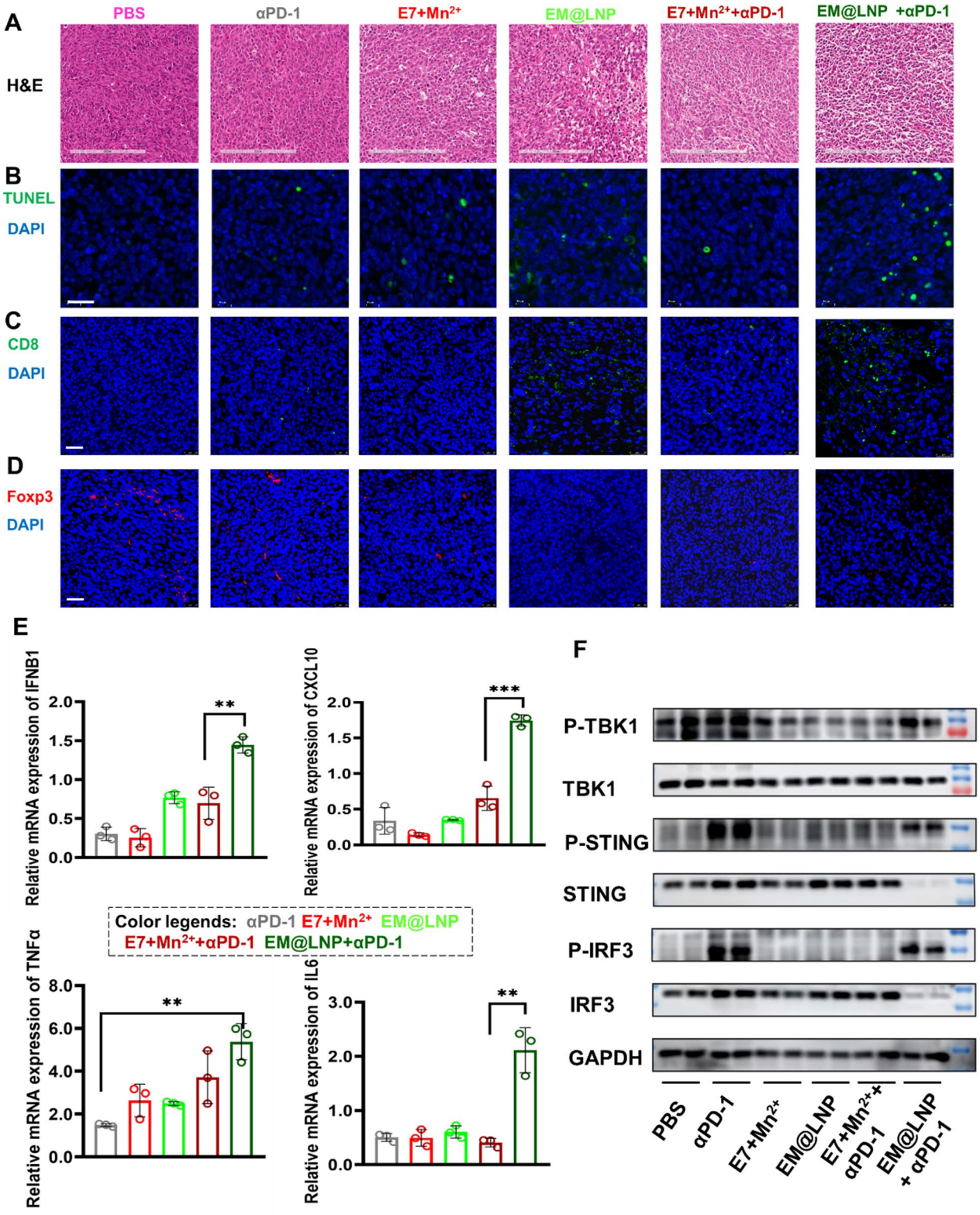

Fig. 5 EM@LNP in combination with iCBT significantly inhibited tumor growth via immune TME modulation. (**A**) H&E images of tumor tissue. (Scale bar: 200 μm). (**B**) TUNEL staining images showing tumor cell apoptosis. (Scale bar: 20 μm). (**C**) Representative IHC images showing infiltration of $CD8^+$ cells in tumor tissue. (Scale bar: 25 μm). (**D**) Representative IHC images showing infiltration of $Foxp3^+$ cells in tumor tissue. (Scale bar: 25 μm). (**E**) RT-PCR results for mRNA levels of immune stimulatory cytokines and chemokines in the tumor tissue. (**F**) Protein expression levels related to the cGAS-STING signaling pathway in tumor tissue after different treatments. Data are presented as mean ± SD. Statistical significances between every two groups were calculated via one-way ANOVA. $^*p < 0.05$, $^{**}p < 0.01$, $^{***}p < 0.001$

profile of EM@LNP both as a standalone treatment and in combination with αPD-1.

EM@LNP combining iCBT adjuvant therapy suppressed postoperative tumor recurrence

Surgical resection is one of the main methods for treating solid tumors, which involves removing tumor tissues to achieve a cure or control the growth of the tumor. However, even with thorough surgical removal, there is still a possibility of tumor recurrence and metastasis in some cases. This poses challenges to clinical treatment as recurrence and metastasis often require more intense and prolonged therapies, making it more difficult to achieve ultimate cure. In order to evaluate the efficacy of EM@LNP immunotherapy alone or in combination with iCBT for postoperative recurrence, a subcutaneous model of postoperative recurrence was used. When the tumor volume reached approximately 200 mm^3, most of the tumor tissue was surgically removed from mice and drug intervention was given before the tumor regrew (Fig. 6A). The results showed that combined iCBT significantly inhibited postoperative recurrent tumor growth compared to EM@LNP immunotherapy alone (Figs. 6B-E) and effectively prolonged mouse survival (Figure S19). These results suggest that in certain situations, combinational iCBT with vaccination can achieve better treatment outcomes than using a single approach and help reduce the risk of tumor recurrence.

Tumor growth following surgical intervention is linked to intricate local inflammatory responses, which are typified by oxygen deprivation and the recruitment of myeloid cells, coupled with a reduction in CTLs, collectively foster a developmentally conducive environment for an immuno-suppressive TME and facilitating the evasion of immunosurveillance by residual tumor cell. IHC staining analysis of immune cell infiltration in post-treated tumor tissues can observe the impact of different treatment approaches on the immune environment within tumor. In contrast to PBS and free EM@LNP groups, H&E staining identified substantial nuclear dissolution and regions of apoptosis within the EM@LNP + αPD-1 immunotherapy group, while TUNEL assay showed the highest rate of DNA damage in this group (Fig. 7A-B). Additionally, $CD8^+$ T cells increased while Tregs ($Foxp3^+$) decreased within the tumor (Fig. 7C-D), and postoperative recurrent tumors had more Tregs ($Foxp3^+$) cells than normal tumor tissues, signifying that surgical treatment can engender a more suppressive immune microenvironment. The combination therapy of EM@LNP + αPD-1 effectively suppressed Tregs cells in tumor lymphocytes and increased the frequency of $CD8^+$ cells and CTLs (Figure S20).

A deeper examination of the systemic cellular immune response revealed that integration of iCBT significantly amplified the overall reaction of critical effector cells in immunized mice. This therapeutic approach not only restored effective T cell function in mice, but also promoted the maturation of CTL or T_{CM} cells (Fig. 6F-G). When contrasted with the control group of mice immunized with EM@LNP alone, combined iCBT markedly enhanced the overall response of key effector cells in immunized mice. In addition, in the PBS group, MDSCs and Tregs were severalfold higher than those in the non-surgical PBS group (Fig. 6F-G). This indicates that surgical treatment leads to pronounced immune suppression within TME, thereby promoting tumor growth recurrence. However, after EM@LNP combined with iCBT therapy, anti-tumor effectors shifted towards a more significant systemic immune response inducing T_{CM} generation which prevented tumor recurrence (Fig. 6B-E, S21). Additionally, analogous immune responses were noted in lymph node cells compared to spleen cells (Fig. 6F, S22). These findings provide valuable insights into the use of EM@LNP combined with iCBT for managing postoperative tumor recurrence and offer novel perspectives on curbing tumor resurgence.

The host cGAS-STING activation is vital for combined vaccination with iCBT

Finally, in order to further investigate the mechanism of action of the cGAS-STING signaling pathway in EM@LNP-mediated combination immunotherapy, experiments were conducted using a TC-1 tumor-bearing model in STING knockout mice treated with E7@LNP + αPD-1 and EM@LNP + αPD-1 treatments (Fig. 8A). In general, in the monotherapy iCBT group, the nanovaccine maintained some inhibitory effect on tumor growth, but not as pronounced as described above for wild-type mice. It is worth noting that the suppressive effect of EM@LNP + αPD-1 was marginally worse than that of E7@LNP + αPD-1 group, primarily characterized by a more rapid increase in tumor volume and weight (Figs. 8B-D). This is because the lack of STING protein in mice prevents Mn^{2+} from functioning properly, diminishing the efficacy of the treatment and even resulting in poorer tumor suppression compared to groups without Mn^{2+}. This indirectly proves that the therapeutic efficacy of this Mn^{2+}-adjuvanted LNP vaccination for tumor immunotherapy relies on the activation of the host STING. In addition, immune cell infiltration and TME showed varying degrees of changes. Specifically, compared with E7@LNP + αPD-1, the frequency of $CD8^+$ cells in splenocytes were reduced in EM@LNP + αPD-1 group but without statistically significant difference, and so was the frequency of CTLs in $CD8^+$ cells (Fig. 8E, S24). Similar results were obtained in lymph nodes (Fig. 8F, S25). This implies that STING agonist Mn^{2+}, as an adjuvant, can enhance the potency of tumor immunotherapy

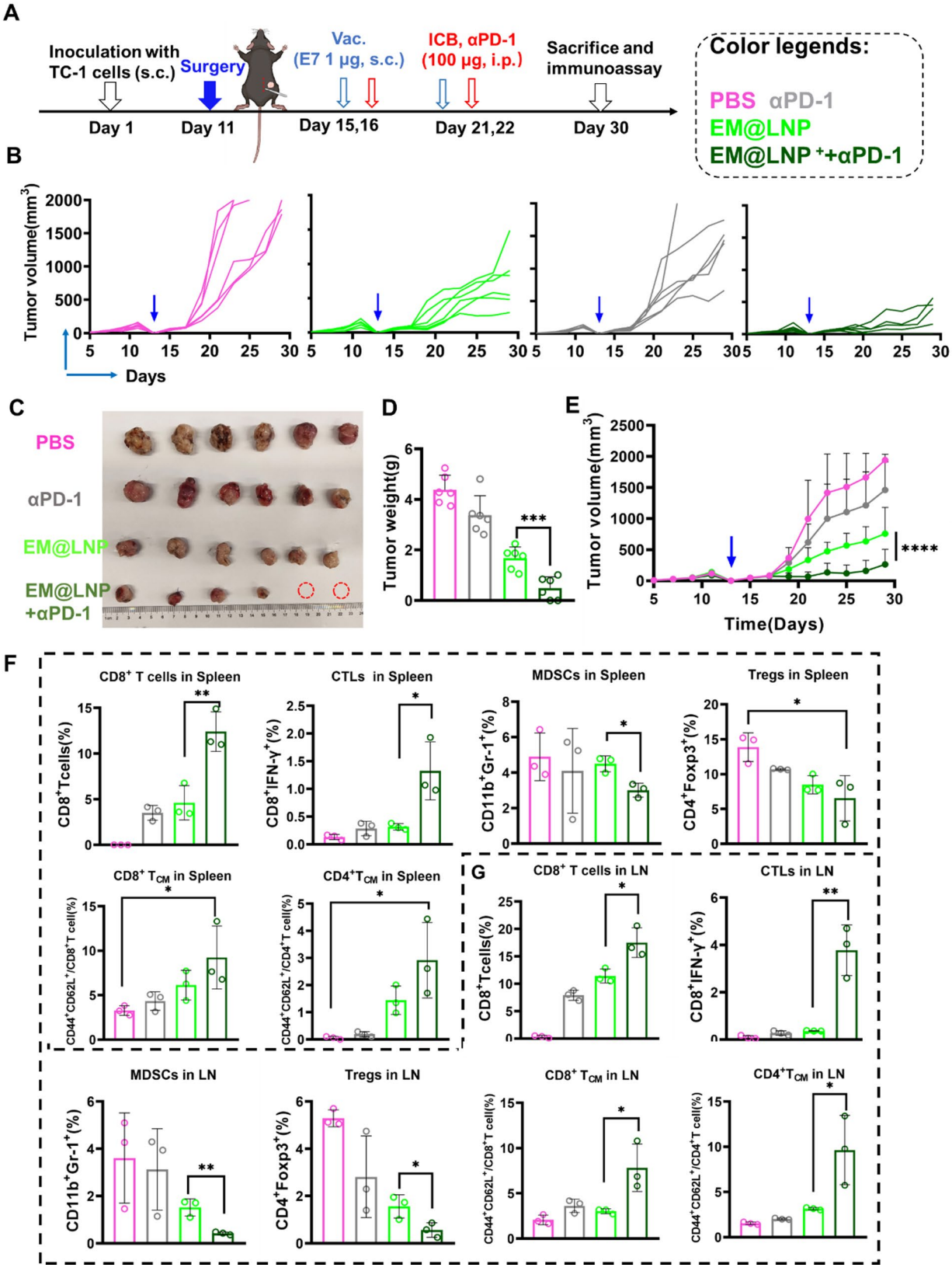

Fig. 6 (See legend on next page.)

(See figure on previous page.)

Fig. 6 EM@LNP combined with iCBT for the treatment of postoperative recurrent tumors. (**A**) The schematic illustration outlining the sequence of drug administration and assays. (**B**) Tumor growth curve in all groups. ($n = 6$). (**C**) The photographs of the tumor obtained at the therapeutic endpoint with various treatments. (**D**) Tumor weight of mice. (**E**) Tumor growth curve of mice. (**F**) Flow cytometric analysis graph of immune cells in the spleen including $CD8^+$T cells, CTLs ($CD8^+IFN\text{-}\gamma^+$), MDSCs ($CD11b^+Gr\text{-}1^+$), Tregs ($CD4^+Foxp3^+$), $CD8^+$ T_{CM} ($CD8^+CD44^+CD62^+$), and $CD4^+$ T_{CM} ($CD4^+CD44^+CD62^+$) cells. And (**G**) in the lymph nodes. Data are presented as mean ± SD. Statistical significances between every two groups were calculated via one-way ANOVA. $^*p < 0.05$, $^{**}p < 0.01$, $^{***}p < 0.001$

by influencing the generation of $CD8^+$ T cells and T_{CM}. Conversely, when performing EM@LNP combined with iCBT under conditions lacking STING protein, it significantly weakened the anti-tumor effect and reduced $CD8^+$ T cells and CTL production accordingly (Figure S23). Consequently, these experimental outcomes underscore the essential function of STING protein plays an indispensable role in enhancing tumor immunotherapy through activation of cGAS-STING pathway by Mn^{2+}.

Discussion

In this work, freeze-dried LNPs (EM@LNP) were prepared for targeted delivery of antigen and Mn^{2+}, and the lyophilized powder subject to reconstitution did not alter the structure and stability of LNP significantly, ensuring endured storage and convenience applications (Scheme 1). The LNPs significantly enhanced the cellular uptake of the E7 antigen. Under low dosage administration, no significant toxicity was observed in cells (Fig. 2A). These findings suggest that the lyophilized LNP is a viable pharmaceutical delivery system, capable of effectively transporting vaccine components, thereby ensuring functional exertion of vaccinations in subsequent investigations.

In vitro studies validated EM@LNP exhibits the strongest activation ability for BMDCs by analyzing the changes in APC function and antigen processing ability after the stimulation of STING agonist: Mn^{2+}. The expression levels of CD86, CD80, CD40, and MHCII markers showed a significant increase, indicating the augmenting expression levels of these mature markers in DC cells (Fig. 2D-G). In addition, the secretion levels of cytokines including TNF-α, IL-1β, IFN-γ, and IFN-β1 also increased in the presence of Mn^{2+} (Fig. 2H-K). Western blot experiments confirmed that EM@LNP upregulated cGAS-STING pathway proteins in both BMDCs and TC-1 cells, however, the activation effect was abolished when STING inhibitor H-151 was added (Fig. 2L-M).

EM@LNP demonstrates superior efficacy as a prophylactic vaccine for in vivo anti-tumor activity compared to E7 antigen alone, indicating a synergistic effect from the incorporation of Mn^{2+}. Flow cytometry analysis of the immune response within the TME revealed an increase in $CD8^+IFN\gamma^+$ T cells and T_{CM} cells in mice treated with E7@LNP compared to those treated with E7 alone (Fig. 3E-F). Notably, the physical mixture of E7 and Mn^{2+} elicited a stronger immune response than the E7@LNP group, while the EM@LNP group exhibited the strongest immune response, suggesting effective stimulation of tumor-infiltrating lymphocytes (TILs) and triggering a potent anti-tumor immune response. In this study, another intriguing finding shows that even the minimal dose of 0.1 μg provided measurable prophylactic benefits by reducing tumor occurrence (Figure S26). Although this lowest dose did not completely inhibit tumor growth, it underscores the promising dose-sparing potential of our formulation. Future studies will further optimize the antigen dose to strike an ideal balance between robust immune activation and minimal antigen load, enhancing clinical applicability and safety.

The incorporation of Mn^{2+} has been found to induce inflammatory changes within the TME and modulated the gene expression profiles of specific immune cell subsets, a process that is pivotal for linking the cross-presentation of tumor antigens with the innate and adaptive immune systems [45]. Consistent with this, in vivo experiments have shown that tumors treated with Mn^{2+} elicit stronger immune responses to iCBT without incurring substantial toxicity (Fig. 4E-F). The data indicate that the LNP formulation significantly enhances the generation and persistence of effector memory T cells, which are critical for long-term antitumor immunity. Moreover, the superior modulation of the immune tumor microenvironment by EM@LNP, as evidenced by comprehensive histopathological and molecular analyses, underscores its potential to synergize more effectively with immune checkpoint blockade therapy compared to the free antigen-adjuvant mixture. A successful response to iCBT is contingent upon the robust interaction between DCs and T cells, the inadequate maturation of DCs and limited infiltration of CTLs can significantly impede the effectiveness of iCBT. It's characterized that STING signaling can activate APCs and produce chemokines and cytokines [46], which can attract a greater number of CTL and then initiates CTL responses within TME, as depicted in Fig. 6I-J, suggesting that this strategy can be further refined as a therapeutic regimen to transform more of immune-cold cancers to be sensitive to iCBT.

Surgical intervention continues to be the mainstay of treatment for patients with solid tumors, yet the recurrence of tumors frequently diminishes their long-term survival rates [47]. Post-surgical physiological alterations, particularly inflammation and immune suppression associated with wound healing, can significantly diminish the effectiveness of tumor immunotherapy and

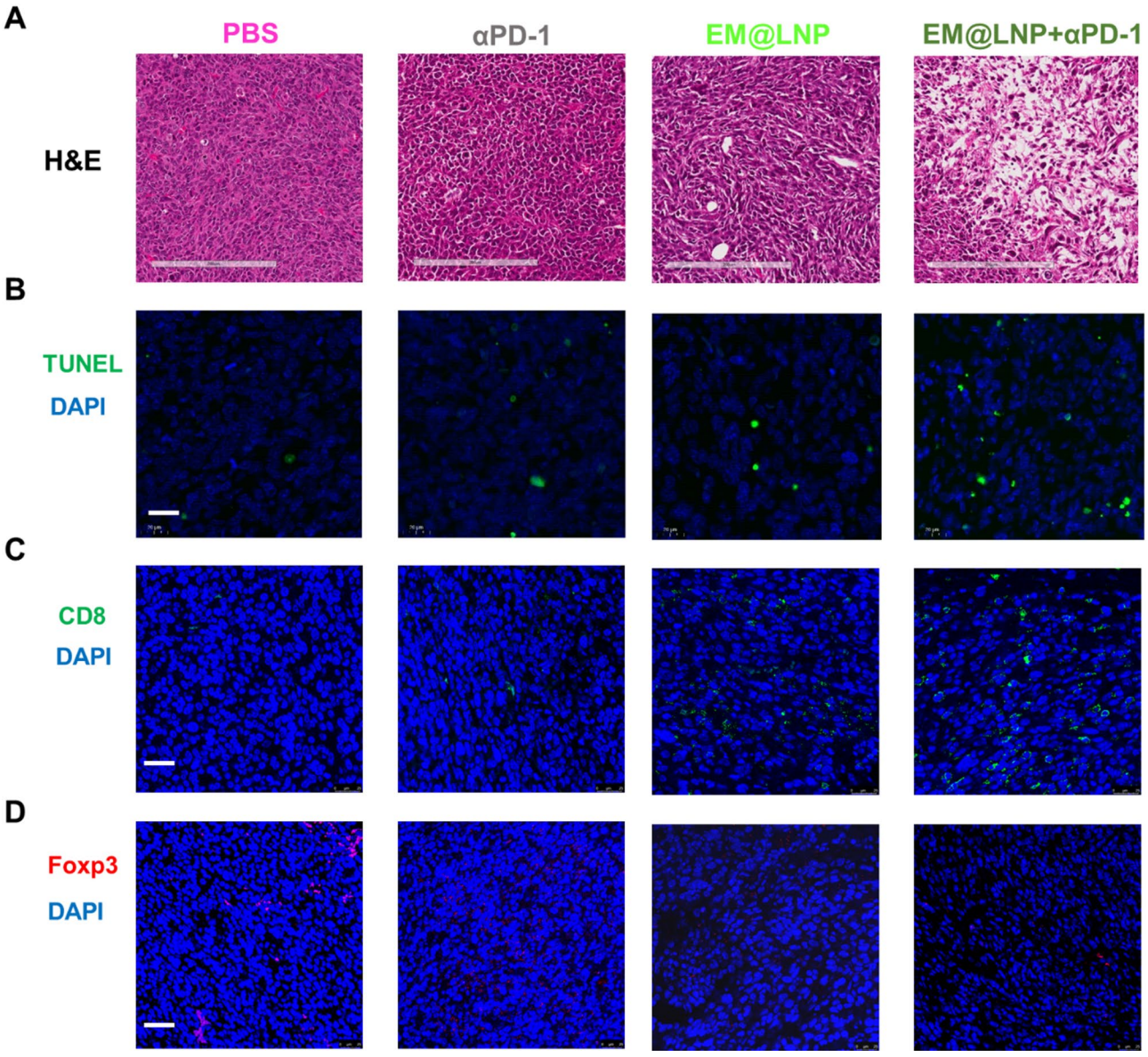

Fig. 7 Tumor tissue H&E and IHC profile of the EM@LNP and/or iCBT treatment in postoperative recurrent tumors. (**A**) H&E histological image of tumor tissue. (Scale bar: 200 μm). (**B**) TUNEL staining image showing tumor cell apoptosis. (Scale bar: 20 μm). (**C**) Representative IHC image of infiltrating $CD8^+$ T cells in tumor tissue. (Scale bar: 25 μm). (**D**) Representative IHC image of infiltrating $Foxp3^+$ T cells in tumor tissue. (Scale bar: 25 μm)

lead to a reduced clinical response to immunotherapy [48]. Inflammatory cells, particularly macrophages represented by M2-type macrophages, are instrumental in the healing and repair of tissues following surgery [49]. Additionally, tumor-associated macrophages secrete anti-inflammatory factors such as IL-10, fostering an immunosuppressive environment that enables residual tumor cells to evade immune detection and accelerates tumor recurrence and metastasis [50]. In vivo models of subcutaneous cervical cancer have demonstrated that the combination of EM@LNP with αPD-1 is the most potent strategies against cancer recurrence (Fig. 6), combined whether used isolation or in combination with ICIs. Specifically, the combination therapy group showed a significant increase in the percentage of tumor-infiltrating CTLs (Figs. 6F-G, S20). Concurrently, there was a significant reduction in the immunosuppressive cell populations, compared to other groups (including anti-PD-1 monotherapy and EM@LNP) as well as MDSCs from untreated surgical cases (Figs. 6F-G; S21-S22). It is noteworthy that the combination therapy group also displayed a substantial increase in the numbers of antigen-specific memory T cells, which can offer enduring protection against tumor recurrence (Figs. 6F-G, S21-S22).

It is important to understand the mechanism how the therapeutic vaccine EM@LNP synergized with immune

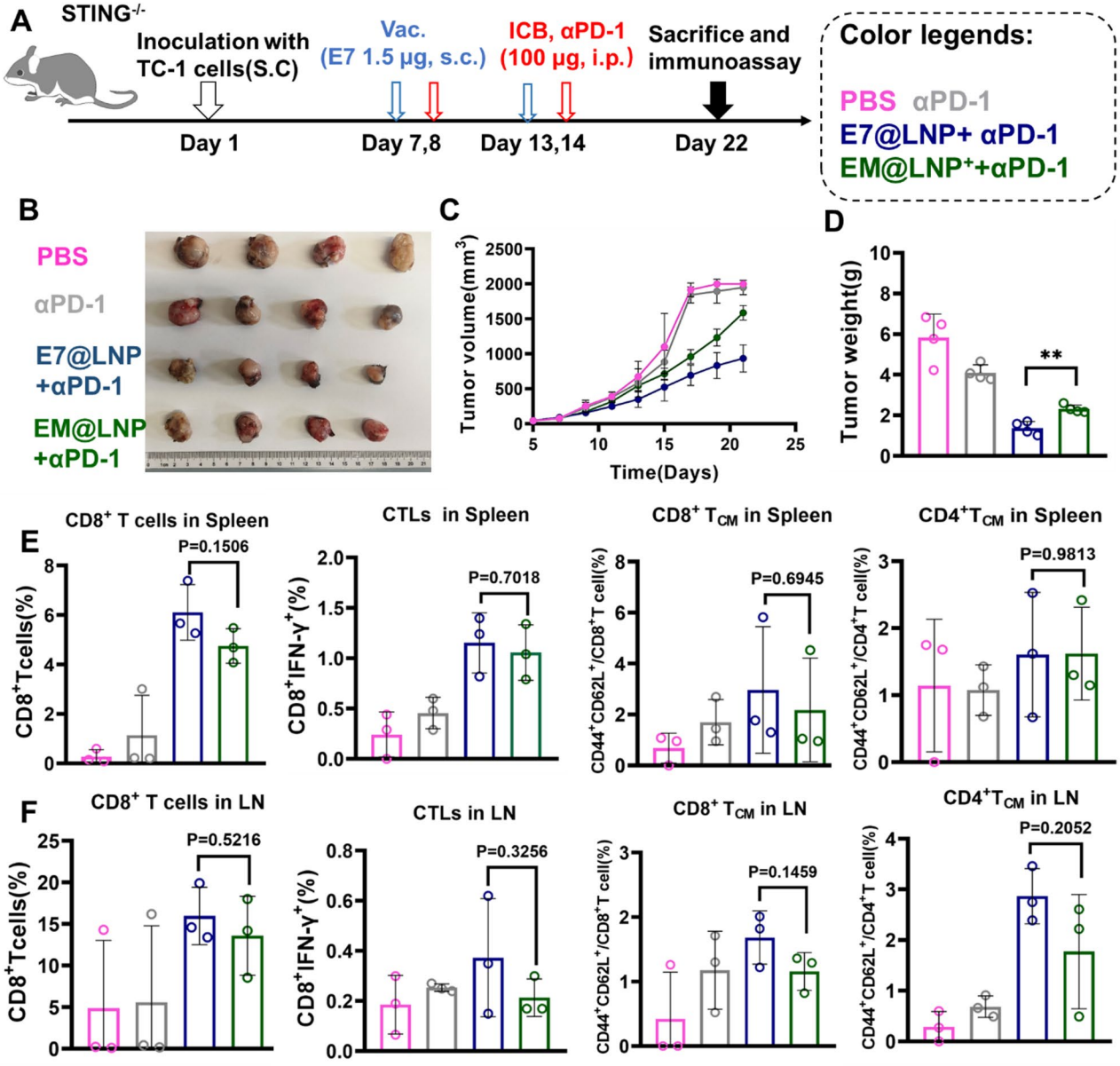

Fig. 8 Vaccinations and combinational iCBT in STING knockout mice. (**A**) The schematic illustration outlining the sequence of drug administration and assays. (**B**) The images of the tumor obtained at the therapeutic endpoint. ($n = 4$) (**C**) Tumor growth curve of mice. (**D**) Tumor weight of the mice. (**E**) Flow cytometry analysis of immune cells in the spleen, including $CD8^+$T cells, CTLs ($CD8^+IFN\text{-}\gamma^+$), $CD8^+$ T_{CM} ($CD8^+CD44^+CD62^+$), and $CD4^+$ T_{CM} ($CD4^+CD44^+CD62^+$) cells and (**F**) lymph nodes. Data are presented as mean ± SD. Statistical significances between every two groups were calculated via one-way ANOVA. $^*p < 0.05$, $^{**}p < 0.01$, $^{***}p < 0.001$

checkpoint inhibitor in tumor treatment. This study further confirmed the pivotal role of the Mn^{2+} induced STING activation in the response to EM@LNP + αPD-1 using STING-deficient mice tumor-bearing model (Fig. 8B-D). It was observed that systemic co-delivery of the Mn^{2+} agonists along with αPD-1 (EM@LNP + αPD-1) did not induce significant augmented effects of anti-tumor T cells and central memory T cells in the spleen and lymph nodes (Fig. 8F-G), when compared to the group (E7@LNP + αPD-1) without adding Mn^{2+} agonists. Nevertheless, even the tumor growth curves and final tumor weights of each group (Fig. 8C-D) demonstrate more tumor suppression of the E@LNP + αPD-1 (without Mn^{2+}) treated $STING^{-/-}$ mice, compared to other treatments including the EM@LNP + αPD-1 (with Mn^{2+}). This suggests that the host STING, rather than intrinsic STING in tumor cells, is essential for the enhanced anti-tumor activity of systemic delivery of STING agonists combined with iCBT therapy. These findings hold potential clinical significance as many solid tumors experience STING deficiency during tumor progression [51], which could provide strategies for future that it's necessary to

stimulate the STING of the cancer patients when conducting the combinational iCBT.

The concept is to selectively activate the cGAS-STING pathway in immune organs and tumors, enhance the presentation of the E7 antigen by APCs, stimulate effector T cells, reverse the suppressive TME, and augment iCBT. Therefore, this method offers a promising avenue for the modulation of TME that can enhance the sensitivity to iCBT and potentially provide additional clinical benefits for cancer patients. Importantly, post-surgery tumor recurrence is a significant challenge that threatens the survival terms of patients due to the deteriorative TME and irresponsive to many therapies. To improve this situation via tuning TME and sensitizing iCBT, Mn^{2+} adjuvanted cancer vaccination based on STING activation may offer innovative strategies for neoadjuvant or adjuvant immunotherapy, before or after tumor surgery, respectively [52]. Recent studies developed Mn^{2+}-based liposomal systems for cGAS-STING activation in cancer immunotherapy. For instance, PL/APMP-DOX liposome-based nanoparticles combine doxorubicin with Mn^{2+} to induce DNA damage and immune activation but are constrained by their reliance on chemotherapy [53]. Similarly, Lipo-MGN nanoparticles address tumor hypoxia to enhance radiotherapy efficacy but lack engagement with adaptive immunity, making them less effective for addressing tumor recurrence [36]. The Mn@mRNA-LNP vaccine [37], which co-delivers mRNA and Mn^{2+}, stimulates robust immune responses and synergizes with iCBT but requires ultra-cold storage due to its liquid formulation, limiting its clinical translation. In contrast, our lyophilized EM@LNP vaccine, which co-delivers the E7 antigen peptide and Mn^{2+}, not only overcomes the storage challenges associated with liquid formulations but also effectively modulates the TME, enhances antigen presentation, and prevents tumor recurrence when combined with iCBT. This lyophilized approach represents an innovative and practical strategy for neoadjuvant or adjuvant immunotherapy, offering significant advantages in stability, scalability, and clinical applicability.

Conclusion

In summary, this study developed EM@LNP, a tumor vaccine co-delivering the E7 antigen and STING agonist Mn^{2+} to generate specific cervical cancer immunity. The Mn^{2+} stimulates DCs and activates the cGAS-STING signaling pathway, enhancing T cell activation and infiltration to strengthen systemic anti-tumor immunity, sensitize iCBT, and suppress tumor growth. Cellular experiments confirmed Mn^{2+}'s role in promoting DC maturation, while mechanistic investigations demonstrated cGAS-STING activation. In TC-1 tumor-bearing mice, EM@LNP vaccination increased infiltration of pro-inflammatory immune cells, significantly inhibited tumor growth, and showed enhanced therapeutic efficacy when combined with αPD-1, without inducing systemic toxicity. Moreover, EM@LNP with αPD-1 effectively suppressed postoperative tumor recurrence and alleviated the suppressive TME. This LNP vaccine and iCBT combinational strategy demonstrates potential for addressing solid tumor recurrence after surgery and offers prospects for treating other malignancies.

Abbreviations

LNP	Lipid Nanoparticle
iCBT	Immune checkpoint blockade therapy
ICB	Checkpoint blockade
DCs	Dendritic Cells
APCs	Antigen Presenting Cells
DSPC	Distearoyl Phosphatidylcholine
Chol	Cholesterol
PC	Phosphatidylcholine
PBS	Phosphate Buffered Saline
FBS	Fetal Bovine Serum
CCK8 kit	Cell Counting Kit-8
TEM	Transmission Electron Microscope
CLSM	Laser Scanning Microscopy
ELISA	Enzyme-Linked Immunosorbent Assay
IHC	Immunohistochemistry
IF	Immunofluorescence
H&E	Hematoxylin and Eosin
TG	Thermogravimetric
TILs	Tumor-Infiltrating Lymphocytes
TME	Tumor Microenvironment
T_{CM}	Central memory T cells
MDSCs	Myeloid-Derived Suppressor Cells
Tregs	Regulatory T cells

Supplementary Information

The online version contains supplementary material available at https://doi.org/10.1186/s12951-025-03445-4.

Supplementary Material 1

Acknowledgements

We thank Dr. Cunbao Liu from the Institute of Medical Biology, Chinese Academy of Medical Sciences (IMBCAMS) for gifting the $STING^{-/-}$ mice.

Author contributions

W. Chen, W. Deng and Z. Song contributed to the conception of this study and funding acquisition. Y. Yang, J. Guo, J. Qi, W. Deng, Y. Zhou, J. Hu, M.H. Hasan did the experiments and data analysis. Y. Yang, J. Guo, J. Qi drafted the manuscript. F. Deng provided comments to methodology and writing. Y. Zhou, M.H. Hasan, W. Chen, W. Deng and Z. Song reviewed and revised the manuscript. All authors have approved the published version of the manuscript.

Funding

This work was supported by the National Natural Science Foundation of China (Nos. 82460111, 82400017, 82360120), Guangdong Provincial Basic Science Fund (No. 2023A1515110028), Yunnan Fundamental Basic Research Project (202301AT070034), the High-level University Construction Fund (06-445-1122), the Open Project of State Key Laboratory of Respiratory Disease (SKLRD-OP-202409), Yunnan Health training project of high level talents (No. H-2024064), Yunnan Outstanding Physician Scheme (KH-SWR-MY-2019-009), the Kunming Medical University Joint Special Project on Applied Basic Research (202301AY070001-210), and the Yunnan High-Level Personnel Support Program (2022-KHRCBZ-B03, KHYJ-2023-05-01). Dr. Chen thanks the Pearl River Rising Scholar Fellowship.

Data availability

No datasets were generated or analysed during the current study.

Declarations

Ethics approval and consent to participate
All the animal studies have been approved by the Guangzhou Medical University IACUC under the ethics approval GY-2022-188.

Consent for publication
All authors agree with the content of the manuscript.

Competing interests
The authors declare no competing interests.

Author details
[1]The NMPA and State Key Laboratory of Respiratory Disease, School of Pharmaceutical Sciences, Department of Emergency, the Second Affiliated Hospital, Guangzhou Medical University, Guangzhou 511436, P. R. China
[2]Yunnan Digestive Endoscopy Clinical Medical Center, Department of Gastroenterology, The First People's Hospital of Yunnan Province, Affiliated Hospital of Kunming University of Science and Technology, Kunming 650032, P. R. China
[3]Graduate School of Biomedical Engineering, ARC Centre of Excellence in Nanoscale Biophotonics, Faculty of Engineering, UNSW Sydney, Sydney, NSW 2052, Australia
[4]School of Biomedical Engineering, University of Technology Sydney, Ultimo, NSW 2007, Australia

Received: 16 January 2025 / Accepted: 5 May 2025
Published online: 26 May 2025

References

1. Lahiri A, Maji A, Potdar PD, Singh N, Parikh P, Bisht B, Mukherjee A, Paul MK. Lung cancer immunotherapy: progress, pitfalls, and promises. Mol Cancer. 2023;22(1):40.
2. Waldman AD, Fritz JM, Lenardo MJ. A guide to cancer immunotherapy: from T cell basic science to clinical practice. Nat Rev Immunol. 2020;20(11):651–68.
3. DePeaux K, Delgoffe GM. Metabolic barriers to cancer immunotherapy. Nat Rev Immunolo. 2021;21(12):785–97.
4. Zhang J, Huang D, Saw PE, Song E. Turning cold tumors hot: from molecular mechanisms to clinical applications. Trends Immunol. 2022;43(7):523–45.
5. Hou AJ, Chen LC, Chen YY. Navigating CAR-T cells through the solid-tumour microenvironment. Nat Rev Drug Discovery. 2021;20(7):531–50.
6. Seder RA, Darrah PA, Roederer M. T-cell quality in memory and protection: implications for vaccine design. Nat Rev Immunol. 2008;8(4):247–58.
7. Li S, Simoni Y, Zhuang S, Gabel A, Ma S, Chee J, et al. Characterization of neoantigen-specific T cells in cancer resistant to immune checkpoint therapies. Proc Natl Acad Sci. 2021;118(30).
8. Wang R, Pan W, Jin L, Huang W, Li Y, Wu D, Gao C, Ma D, Liao S. Human papillomavirus vaccine against cervical cancer: opportunity and challenge. Cancer Lett. 2020;471:88–102.
9. Mousavi T, Valadan R, Rafiei A, Abbasi A, Haghshenas MR. A novel Recombinant protein vaccine containing the different E7 proteins of the HPV16, 18, 6, 11 E7 linked to the HIV-1 Tat (47–57) improve cytotoxic immune responses. Biotechnol Lett. 2021;43:1933–44.
10. Roman A, Munger K. The papillomavirus E7 proteins. Virology. 2013;445(1–2):138–68.
11. Saxena M, van der Burg SH, Melief CJ, Bhardwaj N. Therapeutic cancer vaccines. Nat Rev Cancer. 2021;21(6):360–78.
12. Xiong D, Zhang L, Sun Z-J: Targeting the epigenome to reinvigorate T cells for cancer immunotherapy. Mil Med Res. 2023;10:59.
13. Ruf B, Greten TF, Korangy F. Innate lymphoid cells and innate-like T cells in cancer—at the crossroads of innate and adaptive immunity. Nat Rev Cancer. 2023;23(6):351–71.
14. Sanz-Ortega L, Portilla Y, Pérez-Yagüe S, Barber DF: magnetic targeting of adoptively transferred tumour-specific nanoparticle-loaded CD8(+) T cells does not improve their tumour infiltration in a mouse model of cancer but promotes the retention of these cells in tumour-draining lymph nodes. J Nanobiotechnol. 2019;17:87.
15. Horst AK, Kumashie KG, Neumann K, Diehl L, Tiegs G. Antigen presentation, autoantibody production, and therapeutic targets in autoimmune liver disease. Cell Mol Immunol. 2021;18(1):92–111.
16. Hopfner K-P, Hornung V. Molecular mechanisms and cellular functions of cGAS–STING signalling. Nat Rev Mol Cell Biol. 2020;21(9):501–21.
17. Zhang X, Bai X-c, Chen ZJ. Structures and mechanisms in the cGAS-STING innate immunity pathway. Immunity. 2020;53(1):43–53.
18. Jiang M, Chen P, Wang L, Li W, Chen B, Liu Y, Wang H, Zhao S, Ye L, He Y. cGAS-STING, an important pathway in cancer immunotherapy. J Hematol Oncol. 2020;13:1–11.
19. Cimprich KA, Li G-M, Demaria S, Gekara NO, Zha S, Chen Q. The crosstalk between DNA repair and immune responses. Mol Cell. 2023;83(20):3582–7.
20. Jneid B, Bochnakian A, Hoffmann C, Delisle F, Djacoto E, Sirven P, Denizeau J, Sedlik C, Gerber-Ferder Y, Fiore F. Selective STING stimulation in dendritic cells primes antitumor T cell responses. Sci Immunol. 2023;8(79):eabn6612.
21. Li W, Lu L, Lu J, Wang X, Yang C, Jin J, et al. cGAS-STING-mediated DNA sensing maintains CD8 (+) T cell stemness and promotes antitumor T cell therapy. Sci Transl Med. 2022;12(549).
22. Pan B-S, Perera SA, Piesvaux JA, Presland JP, Schroeder GK, Cumming JN, Trotter BW, Altman MD, Buevich AV, Cash B. An orally available non-nucleotide STING agonist with antitumor activity. Science. 2020;369(6506):eaba6098.
23. Yang Y, Qi J, Hu J, Zhou Y, Zheng J, Deng W, Inam M, Guo J, Xie Y, Li Y, Xu C, Deng W, Chen W. Lovastatin/SN38 co-loaded liposomes amplified ICB therapeutic effect via remodeling the immunologically-cold colon tumor and synergized stimulation of cGAS-STING pathway. Cancer Lett. 2024;588:216765.
24. Zhang K, Qi C, Cai K. Manganese-based tumor immunotherapy. Adv Mater. 2023;35(19):2205409.
25. Nicolai CJ, Wolf N, Chang IC, Kirn G, Marcus A, Ndubaku CO, et al. NK cells mediate clearance of CD8 (+) T cell-resistant tumors in response to STING agonists. Sci Immunol. 2020;5(45):eaaz2738.
26. Bråve A, Ljungberg K, Wahren B, Liu MA. Vaccine delivery methods using viral vectors. Mol Pharm. 2007;4(1):18–32.
27. Bolhassani A, Safaiyan S, Rafati S. Improvement of different vaccine delivery systems for cancer therapy. Mol Cancer. 2011;10:1–20.
28. Meng J, Zhang P, Chen Q, Wang Z, Gu Y, Ma J, Li W, Yang C, Qiao Y, Hou Y. Two-Pronged intracellular Co-Delivery of antigen and adjuvant for synergistic Cancer immunotherapy. Adv Mater. 2022;34(21):2202168.
29. Hou Y, Wang Y, Tang Y, Zhou Z, Tan L, Gong T, Zhang L, Sun X. Co-delivery of antigen and dual adjuvants by aluminum hydroxide nanoparticles for enhanced immune responses. J Controlled Release. 2020;326:120–30.
30. Guo J, Gu M, Chen Y, Xiong T, Zhang Y, Chen S, et al. Nucleic acid delivery by lipid nanoparticles for organ targeting. Chin Chem Lett. 2025: 110849.
31. Albertsen CH, Kulkarni JA, Witzigmann D, Lind M, Petersson K, Simonsen JB. The role of lipid components in lipid nanoparticles for vaccines and gene therapy. Adv Drug Deliv Rev. 2022;188:114416.
32. Zhang R, Wang C, Guan Y, Wei X, Sha M, Yi M, Jing M, Lv M, Guo W, Xu J. Manganese salts function as potent adjuvants. Cell Mol Immunol. 2021;18(5):1222–34.
33. Lv M, Chen M, Zhang R, Zhang W, Wang C, Zhang Y, Wei X, Guan Y, Liu J, Feng K. Manganese is critical for antitumor immune responses via cGAS-STING and improves the efficacy of clinical immunotherapy. Cell Res. 2020;30(11):966–79.
34. Zheng S-J, Yang M, Luo J-Q, Liu R, Song J, Chen Y. Du, Manganese-Based immunostimulatory Metal–Organic framework activates the cGAS-STING pathway for Cancer metalloimmunotherapy. ACS Nano. 2023;17(16):15905–17.
35. Peng C, Zhao M, Wang X, Yan M, Han Y, Chen D, Hu H. Manganese ion gradient liposomes modified by disulfide bond enhance cellular uptake and tumor immunity. Mater Design. 2023;233:112178.
36. Thomas RG, Kim S, Nagareddy R, Vijayan V, Pullickal AM, Yoon MS, Park IK, Jeong YY. Lipo-MGN nanoparticle hypoxia attenuation-mediated single-dose radiotherapy-and pH/ROS-responsive T1 contrast magnetic resonance imaging in hepatocellular carcinoma. Cancer Nanotechnol. 2023;14(1):53.
37. Luo Z, Lin Y, Meng Y, Li M, Ren H, Shi H, Cheng Q, Wei T. Spleen-Targeted mRNA vaccine doped with manganese adjuvant for robust anticancer immunity in vivo. ACS Nano. 2024;18(44):30701–15.
38. Chattergoon MA, Kim JJ, Yang J-S, Robinson TM, Lee DJ, Dentchev T, Wilson DM, Ayyavoo V, Weiner DB. Targeted antigen delivery to antigen–presenting cells including dendritic cells by engineered Fas-mediated apoptosis. Nat Biotechnol. 2000;18(9):974–9.

39. Adams EW, Ratner DM, Seeberger PH, Hacohen N. Carbohydrate-mediated targeting of antigen to dendritic cells leads to enhanced presentation of antigen to T cells. ChemBioChem. 2008;9(2):294–303.
40. Uddin MN, Roni MA. Challenges of storage and stability of mRNA-based COVID-19 vaccines. Vaccines. 2021;9(9):1033.
41. Muramatsu H, Lam K, Bajusz C, Laczkó D, Karikó K, Schreiner P, Martin A, Lutwyche P, Heyes J, Pardi N. Lyophilization provides long-term stability for a lipid nanoparticle-formulated, nucleoside-modified mRNA vaccine. Mol Ther. 2022;30(5):1941–51.
42. van Winden EC, Crommelin DJ. Short term stability of freeze-dried, lyoprotected liposomes. J Controlled Release. 1999;58(1):69–86.
43. Li Y, Zhu R, Guo Y, Wang Y, Ma R, Ma K, et al. Sequential-gated transformable nanoprodrug potentiates antitumor immunity through TME modulation and STING activation. Chin Chem Lett. 2024:110704.
44. Taylor PR, Gordon S, Martinez-Pomares L. The mannose receptor: linking homeostasis and immunity through sugar recognition. Trends Immunol. 2005;26(2):104–10.
45. Deng X, Liu T, Zhu Y, Chen J, Song Z, Shi Z, Chen H. Ca & Mn dual-ion hybrid nanostimulator boosting anti-tumor immunity via ferroptosis and innate immunity awakening. Bioactive Mater. 2024;33:483–96.
46. Wu Y, Tang CA, Mealer C, Bastian D, Hanief Sofi M, Tian L, Schutt S, Choi HJ, Ticer T, Zhang M, Sui X, Huang L, Mellor AL, Hu CA, Yu XZ. STING negatively regulates allogeneic T-cell responses by constraining antigen-presenting cell function. Cell Mol Immunol. 2021;18(3):632–43.
47. Chen Q, Wang C, Zhang X, Chen G, Hu Q, Li H, Wang J, Wen D, Zhang Y, Lu Y, Yang G, Jiang C, Wang J, Dotti G, Gu Z. In situ sprayed bioresponsive immunotherapeutic gel for post-surgical cancer treatment. Nat Nanotechnol. 2019;14(1):89–97.
48. Liu J, Blake SJ, Yong MC, Harjunpää H, Ngiow SF, Takeda K, Young A, O'Donnell JS, Allen S, Smyth MJ, Teng MW. Improved efficacy of neoadjuvant compared to adjuvant immunotherapy to eradicate metastatic disease. Cancer Discov. 2016;6(12):1382–99.
49. Wang Y, Yu J, Luo Z, Shi Q, Liu G, Wu F, et al. Engineering endogenous tumor-Associated Macrophage-Targeted biomimetic Nano-RBC to reprogram tumor immunosuppressive microenvironment for enhanced Chemo-Immunotherapy. Adv Mat. 2021;33(39):e2103497.
50. York AG, Skadow MH, Oh J, Qu R, Zhou QD, Hsieh WY, Mowel WK, Brewer JR, Kaffe E, Williams KJ, Kluger Y, Smale ST, Crawford JM, Bensinger SJ, Flavell RA. IL-10 constrains sphingolipid metabolism to limit inflammation. Nature. 2024;627(8004):628–35.
51. Chelvanambi M, Fecek RJ, Taylor JL, Storkus WJ. STING agonist-based treatment promotes vascular normalization and tertiary lymphoid structure formation in the therapeutic melanoma microenvironment. J Immunother Cancer. 2021;9(2):e001906.
52. Garland KM, Sheehy TL, Wilson JT. Chemical and biomolecular strategies for STING pathway activation in Cancer immunotherapy. Chem Rev. 2022;122(6):5977–6039.
53. Hou L, Tian C, Yan Y, Zhang L, Zhang H, Zhang Z. Manganese-based nanoactivator optimizes cancer immunotherapy via enhancing innate immunity. ACS Nano. 2020;14(4):3927–40.

Publisher's note